

AD A091509

UNCLASSIFIED

SECURITY CLASSIFICATION OF THIS PAGE (When Data Entered)

REPORT DOCUMENTATION PAGE		READ INSTRUCTIONS BEFORE COMPLETING FORM
1. REPORT NUMBER <b>14</b> HDL-TR-1931 ✓	2. GOVT ACCESSION NO. AD-A092 509	3. RECIPIENT'S CATALOG NUMBER
4. TITLE (and Subtitle) <b>6</b> A Near-Surface Burst EMP Driver Package for Prompt Gamma-Induced Sources.		5. TYPE OF REPORT & PERIOD COVERED <b>9</b> Technical Report
7. AUTHOR(s) <b>10</b> William T. Wyatt, Jr.		6. PERFORMING ORG. REPORT NUMBER
9. PERFORMING ORGANIZATION NAME AND ADDRESS Harry Diamond Laboratories 2800 Powder Mill Road Adelphi, MD 20783 ✓		8. CONTRACT OR GRANT NUMBER(s) DA: 1L162120AH25 <b>16</b>
11. CONTROLLING OFFICE NAME AND ADDRESS U.S. Army Materiel Development and Readiness Command Alexandria, VA 22333		10. PROGRAM ELEMENT, PROJECT, TASK AREA & WORK UNIT NUMBERS Prog. El.: 6.21.20.A
14. MONITORING AGENCY NAME & ADDRESS (if different from Controlling Office)		12. REPORT DATE Sep 1980 <b>11</b>
		13. NUMBER OF PAGES <b>12</b> 50
		15. SECURITY CLASS. (of this report) UNCLASSIFIED
		15a. DECLASSIFICATION/DOWNGRADING SCHEDULE
16. DISTRIBUTION STATEMENT (of this Report) Approved for public release; distribution unlimited.		
17. DISTRIBUTION STATEMENT (of the abstract entered in Block 20, if different from Report)		
18. SUPPLEMENTARY NOTES HDL Project: X750E6 DRCMS Code: 612120.H250011		
19. KEY WORDS (Continue on reverse side if necessary and identify by block number) EMP                                      Electromagnetic pulse                      Curve fitting Compton currents                      Radiation transport Nuclear explosions                      Monte Carlo method Gamma rays                                      Computer codes		
20. ABSTRACT (Continue on reverse side if necessary and identify by block number) This report summarizes the development of a software package specifying electromagnetic pulse (EMP) drivers produced by prompt gamma rays emitted by a near-surface nuclear burst in the air. The package is designed for use with the NEMP EMP prediction computer code. This report describes improved calculations of EMP drivers arising from a point gamma source in air over ground, based on Monte Carlo simulation of the gamma transport by the specially		

163050 alt

UNCLASSIFIED

SECURITY CLASSIFICATION OF THIS PAGE(When Data Entered)

20. Abstract (Cont'd)

developed SLEDGE computer code. This simulation was done for seven source gamma energies from 0.5 to 7.0 MeV. The transport was carried to a range of 25 mean free paths. Correlated sampling was used to estimate Compton electron currents more accurately. The theoretical basis of the SLEDGE code is discussed. Analytic approximations to the Monte Carlo results are described in detail, including (1) the energy deposition buildup factor (both free field and ground influenced), (2) time dependence of energy deposition as a function of both range from the burst and nearness to the ground, (3) ratio of radial Compton electron current to energy deposition rate, and (4) theta Compton electron current due to the presence of the ground. Comparisons are made with two previous EMP driver packages, with good agreement for cases where the previous packages are believed reliable.

FOREWORD

The nuclear electromagnetic pulse (EMP) is a transient broadband electromagnetic field capable of damaging or upsetting electronic equipment on the tactical nuclear battlefield. To predict the signature of the EMP generated by a nuclear burst, it is necessary to determine the EMP drivers--time and space varying ionization and Compton electron currents in the nuclear radiation field around the burst. Once the ionization and Compton currents are specified, it is usually possible to solve some form of Maxwell's equations for the EMP generated.

This report summarizes the development of a software package specifying EMP drivers produced by prompt gamma rays emitted by a near-surface burst in the air. The package was designed for use with the NEMP EMP environment prediction computer code used at the Harry Diamond Laboratories. A separate report, A Near-Surface Burst EMP Driver Package for Neutron-Induced Sources, HDL-TR-1930 (September 1980), summarizes the development of a similar software package for EMP drivers due to neutrons and neutron-induced secondary gamma rays.

Part I of this report describes the development of the Monte Carlo gamma ray transport computer code and data base to be fitted. Part II describes the curve-fitting exercise and compares these results with earlier results.

Accession For	
NTIS GRA&I	<input checked="" type="checkbox"/>
DTIC TAB	<input type="checkbox"/>
Unannounced	<input type="checkbox"/>
Justification	
By _____	
Distribution/	
Availability Codes	
Dist	Avail and/or
	Special
A	

CONTENTS

	<u>Page</u>
FOREWORD.....	3
PART I. EMP DRIVERS FROM GAMMA TRANSPORT BY MONTE CARLO	
1. REQUIREMENTS FOR NEW EMP DRIVER AND GAMMA TRANSPORT DATA.....	9
2. DEVELOPMENT OF SLEDGE, A MONTE CARLO GAMMA TRANSPORT CODE.....	10
2.1 Random Walk and Estimator Scoring.....	11
2.2 Biasing and Importance Functions.....	13
2.2.1 Source Biasing.....	14
2.2.2 Transport Biasing.....	15
2.2.3 Collision Biasing.....	16
2.3 Cross Sections.....	17
2.4 Scoring EMP Drivers by Correlated Sampling.....	18
3. CALCULATIONS PERFORMED.....	20
3.1 One-Dimensional Studies.....	20
3.2 Two-Dimensional Air-Ground Interface Effects.....	21
PART II. ANALYTICAL FITS TO EMP DRIVER RESULTS	
4. ENERGY DEPOSITION.....	23
4.1 Fitting Free-Field Buildup Factors for Seven Gamma Ray Energies.....	23
4.2 Ground Effect on Buildup Factor.....	24
4.3 Time Dependence of Energy Deposition Rate.....	25
5. RELATION OF COMPTON CURRENT TO ENERGY DEPOSITION RATE.....	29
5.1 Compton Current from First Collisions of Gamma Rays.....	29
5.2 Radial Compton Current from Multiply Scattered Gamma Rays.....	30
5.3 Theta Compton Current from Multiply Scattered Gamma Rays.....	31
6. COMPARISON WITH PREVIOUS RESULTS.....	31
6.1 Buildup Factor for Energy Deposition.....	31
6.2 Time Dependence of Energy Deposition Rate.....	35
6.3 Time Dependence of Radial Compton Current.....	39

CONTENTS (Cont'd)

	<u>Page</u>
7. CONCLUDING REMARKS.....	43
LITERATURE CITED.....	44
DISTRIBUTION.....	45

FIGURES

1 Energy deposition buildup factors compared for 0.5-MeV gamma rays, for range in attenuation lengths.....	32
2 Energy deposition buildup factors compared for 1.5-MeV gamma rays, for range in attenuation lengths.....	33
3 Energy deposition buildup factors compared for 5.0-MeV gamma rays, for range in attenuation lengths.....	33
4 Energy deposition buildup factors compared for 0.5-MeV gamma rays, for range in meters.....	34
5 Energy deposition buildup factors compared for 1.5-MeV gamma rays, for range in meters.....	34
6 Energy deposition buildup factors compared for 5.0-MeV gamma rays, for range in meters.....	35
7 Time dependence of energy deposition buildup factors compared at 300-m range for 0.5-MeV gamma rays.....	36
8 Time dependence of energy deposition buildup factors compared at 300-m range for 1.5-MeV gamma rays.....	36
9 Time dependence of energy deposition buildup factors compared at 300-m range for 5.0-MeV gamma rays.....	37
10 Time dependence of energy deposition buildup factors compared at 3000-m range for 0.5 MeV-gamma rays.....	37
11 Time dependence of energy deposition buildup factors compared at 3000-m range for 1.5-MeV gamma rays.....	38
12 Time dependence of energy deposition buildup factors compared at 3000-m range for 5.0-MeV gamma rays.....	38

FIGURES (Cont'd)

	<u>Page</u>
13 Time dependence compared for ratio of radial Compton electron current to energy deposition rate, at 300-m range for 0.5-MeV gamma rays.....	40
14 Time dependence compared for ratio of radial Compton electron current to energy deposition rate, at 300-m range for 1.5-MeV gamma rays.....	40
15 Time dependence compared for ratio of radial Compton electron current to energy deposition rate, at 300-m range for 5.0-MeV gamma rays.....	41
16 Time dependence compared for ratio of radial Compton electron current to energy deposition rate, at 3000-m range for 0.5-MeV gamma rays.....	41
17 Time dependence compared for ratio of radial Compton electron current to energy deposition rate, at 3000-m range for 1.5-MeV gamma rays.....	42
18 Time dependence compared for ratio of radial Compton electron current to energy deposition rate, at 3000-m range for 5.0-MeV gamma rays.....	42

TABLES

1 Seven Gamma Ray Energies and Attenuation Parameters.....	20
2 SLEDGE Meshes for Two-Dimensional Problems.....	21
3 Energy Deposition Buildup Factor Parameters for $B = 1 + a(r/\lambda)^k$ .....	24
4 Ratio of Radial Compton Electron Current to Energy Deposition for First-Collision Gamma Rays from a Point Source.....	29
5 Fit Parameters for Ratio of Radial Compton Electron Current to Energy Deposition Rate for Multiply Scattered Gamma Rays.....	30

## PART I. EMP DRIVERS FROM GAMMA TRANSPORT BY MONTE CARLO

### 1. REQUIREMENTS FOR NEW EMP DRIVER AND GAMMA TRANSPORT DATA

Electromagnetic pulse (EMP) drivers consist of one component arising from prompt gamma radiation and a second component arising from neutron radiation. The NEMP computer code<sup>1,2</sup> obtains the solution of Maxwell's equations for EMP from a near-surface burst in the air. The EMP drivers must be incorporated into the NEMP code as smooth fits to quasi-analytic or Monte Carlo predictions. Earlier EMP driver fits were used in the LEMP computer code<sup>3</sup> for EMP from surface bursts. The LEMP prompt gamma ray EMP drivers were used in the NEMP code at first, but a quick-look Monte Carlo study by this author confirmed several deficiencies in these LEMP drivers:

a. Incorrect range dependence for the gamma ray buildup factor at more than about five gamma ray attenuation lengths penetration, becoming exponentially worse at deeper penetrations

b. Incorrect time dependence at deeper penetrations (LEMP drivers' time dependence is independent of range and decreases with time too rapidly at deeper penetrations.)

c. Lack of a ground effect on the buildup factor (The ground actually inhibits the increase of the buildup factor with range for observers near the ground.)

d. Lack of late vertical Compton currents induced by the effect of the ground on gamma transport

It was therefore decided to develop newer, more realistic drivers for the NEMP code that would overcome these deficiencies and also account for the effect of a nonzero burst height. The new drivers would be valid to a penetration depth of at least 20 gamma ray attenuation lengths and would encompass more discrete gamma ray energies than the LEMP drivers (which included 0.5-, 1.5-, and 5.0-MeV gamma ray sources). The new drivers would use the same LEMP philosophy of using well-chosen analytic functionals to describe time and space dependence of the data, in preference to using piecewise polynomial fits.

<sup>1</sup>H. J. Longley, C. L. Longmire, and K. S. Smith, Development of NEMP (U), Mission Research Corp., Santa Barbara, CA, HDL-CR-75-001-1 (April 1975). (SECRET--RESTRICTED DATA)

<sup>2</sup>H. J. Longley and K. S. Smith, Developments in NEMP for 1977 (U), Mission Research Corp., Santa Barbara, CA, HDL-CR-77-0022-1 (January 1978). (SECRET--RESTRICTED DATA)

<sup>3</sup>H. J. Longley and C. L. Longmire, Development and Testing of LEMP 1, Los Alamos Scientific Laboratory, NM, LA-4346 (April 1970).

## 2. DEVELOPMENT OF SLEDGE, A MONTE CARLO GAMMA TRANSPORT CODE

To first test the validity of the LEMP drivers and then obtain needed, more detailed predictions of EMP drivers, it was decided to write a special-purpose Monte Carlo code for gamma ray transport, specially tailored for efficiency in calculating the data needed. The code was written in FORTRAN IV and run on the Harry Diamond Laboratories (HDL) computer (an IBM System/370 Model 168). The code consists of several thousand FORTRAN statements and includes 53 program and subprogram units. It was named SLEDGE, after the basic tool for realigning existing structures; "SLEDGE" is also an acronym for "surface and low-altitude EMP drivers due to gamma emission." An overview of the SLEDGE code is presented here with additional detail on innovations or other important aspects.

The SLEDGE code models time-dependent gamma ray transport from a point source in air-over-ground cylindrical geometry. The collision kernel includes Compton scattering, photoabsorption, and pair production. Time dependence is maintained in retarded time from the source point (the nuclear burst). For this study, the gamma ray source was monochromatic in energy and a delta function in time.

The gamma ray flux is sampled to obtain the desired EMP driver response functions--electron current vector and energy deposition rate. Energy deposition and radial and theta components of the electron current vector are scored within volume detectors by both track-length and collision estimators of the gamma ray flux and are scored at the surfaces of volume detectors by a boundary crossing estimator of the gamma ray flux. Optionally, collision estimator scoring can be done in spherical polar coordinate radial bins to obtain one-dimensional (1-d) results. Thus, removal of the ground allows spherically symmetric free-field results to be accumulated in the 1-d radial bins. Inclusion of the ground allows azimuthally symmetric, ground-influenced results to be accumulated in the 2-d cylindrical geometry volume detectors.

The random walk permits exponential transform biasing, angular and energy biasing of the source, and directional biasing of gamma rays emerging from Compton collisions. Splitting can be done to prevent growth of particle weight due to biasing at collisions or at transports. Splitting and roulette can be used in connection with detector importances to improve statistics in desired regions (zone splitting). Splitting and roulette can be used also to reduce the variance of gamma ray weights in specifiable detectors (weight balancing). A special technique may be used to greatly reduce the variance of the ratio of electron current to energy deposition rate, based on the (early time) correlation between the electron currents and the energy deposition.

## 2.1 Random Walk and Estimator Scoring

After reading problem input, setting up time and space meshes, and initializing necessary tables, the SLEDGE code executes a batch loop and then scans the results of each batch to develop grand totals and batch statistics. Each batch consists of a particle (gamma ray) history loop followed by saving the total results for the batch. A typical production run of 30,000 histories might consist of 20 batches of 1500 histories each. Each particle history consists of identifying a particle and all its subparticles created by splitting and following them through successive random walks until extinction. The random walk consists of these steps:

- (1) Generating the particle or subparticle
- (2) Determining the number of mean free paths down which the particle is to be transported prior to a collision
- (3) Tracking the particle through space and time to the collision point, while scoring track-length or surface crossing estimators for the detectors encountered
- (4) Colliding the particle to obtain the emergent particle energy and direction, while scoring collision estimators for the detector involved, and then repeating steps (2), (3), and (4) until extinction

The particle or subparticle can be killed or split after step (2) or (3) or (4) through photoabsorption, escape, age cutoff, low energy cutoff, collision number limit, or any of the roulette or splitting mechanisms. Subparticles produced are stored in a split stack and are withdrawn one at a time from the split stack in step (1). Ultimately, there are no entries remaining in the split stack, and the next particle history can be started.

Many standard techniques were drawn from the literature, particularly from Carter and Cashwell.<sup>4</sup>

Generating the particle involves determining its position (at the burst), direction cosines (usually biased), energy (simply monochromatic in this study), age, and weight.

Determining the number of mean free paths,  $N$ , was done by

$$N = -\ln(\xi)$$

---

<sup>4</sup>L. L. Carter and E. D. Cashwell, *Particle-Transport Simulation with the Monte Carlo Method*, U.S. Energy Research and Development Administration TID-26607 (1975).

for a uniform random number,  $\xi$ , selected from the interval (0,1). A rejection method was used to eliminate escapes before the first scatter for a particle. Both exponential transform and importance function biasing were used for first-scatter transport, and exponential transform biasing was used for later scatters. These are discussed in more detail in section 2.2.

Tracking the particle involved finding its track-length in the detector that it was inside (detector volumes being mutually exclusive and filling all space within the grid outer boundary), scoring track-length and surface crossing estimators, moving the particle to the next detector, and repeating the process until the particle reached a collision point or was killed. When the particle reached a collision point, the 2-d and 1-d collision estimators were scored, also.

Standard means were used to select the collision event from Compton collision, photoabsorption, and pair production probabilities. Pair production was assumed isotropic. Standard algorithms were used to select the emergent energy and the direction of Compton scattered gamma rays. Emergent direction biasing could be used, as described in section 2.2.

The track-length estimation of the flux,  $F$  (that is, path length per unit volume), is

$$F = pW_{BC}/V ,$$

where  $p$  is the track-length in the particular volume detector and time bin,  $W_{BC}$  is the particle weight before collision, and  $V$  is the detector volume. The electron current magnitude,  $J$ , is

$$J = F (R_C/\lambda_C + R_p/\lambda_p) ,$$

where  $R_C$  is the average forward range of Compton electrons (for the incident gamma ray energy),  $\lambda_C$  is the Compton collision or attenuation length,  $R_p$  is the average forward range of photoelectrons, and  $\lambda_p$  is the photoelectric absorption length.  $R_C$  was computed and tabulated by the SLEDGE code by using the Compton differential scattering cross section and the electron range-energy relation in air.  $R_p$  was adapted from the literature. The energy deposition,  $D$ , is

$$D = F [E/\lambda_a + E/\lambda_p + (E - 1.022)/\lambda_{pp}] ,$$

where  $E$  is the gamma ray energy in MeV,  $\lambda_a$  is the Compton absorption length, and  $\lambda_{pp}$  is the pair production absorption length.

Once  $J$  is obtained, it is decomposed into radial and vertical components.

The surface crossing estimation of the flux, scored only when the surface is crossed, is

$$F = W_{BC}/CA ,$$

where C is the sine of the angle between the surface and the particle direction and A is the area of the surface. J and D are derived as before.

The collision estimation of the flux, scored only when a collision point is reached, is

$$F = W_{BC}/\sigma V ,$$

where  $\sigma$  is the total collision cross section in the detector with volume V. J and D are derived as before.

The time bin associated with scoring surface crossing and collision estimators is simple to determine. However, for the track-length estimator, the particle may pass through several time bins while traversing a detector volume. The portion of the track-length spent in each time bin must be determined to score the time dependence properly. Although this determination requires somewhat more computer time, the associated variance is usually much better for the track-length estimator. Generally, all three estimators were used to check for agreement and insure correct results.

No account was taken of the effect of the ground upon the transport of Compton electrons and photoelectrons. Some effects would be expected within roughly 1 m of the ground. This effect could be a fruitful subject for future study.

## 2.2 Biassing and Importance Functions

The analog model of gamma ray transport (that is, no biassing or importance functions) is useless for deep penetration problems. Some means must be used to force gamma rays to penetrate to distant regions in large enough numbers to produce useful, low variance results. A number of methods were tested in the SLEDGE code for the problems under consideration. These may be categorized as (1) source biassing, (2) transport biassing, and (3) collision biassing, modifying respectively the source function, the transport kernel, or the collision kernel of the transport integral. Two risks are associated with the use of properly normalized biassing methods:

a. The variance of the flux may be infinite or possibly very large so that as the number of batches increases, the variance gets larger, not smaller.

b. The transport integral (integrated over position, velocity, time, and energy) may be undersampled since strong biasing may force the sampling away from portions of the integral space that contribute significantly to the correct answer.

Thus, the biasing methods must be properly constructed and not overused and yet must be powerful enough to be worth the trouble of using. In general, source biasing very effectively reduces the variance in deep penetration problems. Also, splitting with roulette is a simple but highly effective method for transport biasing. In this study, collision biasing was only of minor importance in variance reduction.

### 2.2.1 Source Biasing

Source directional biasing was not used in the SLEDGE code to obtain 1-d results. However, for the 2-d air-over-ground studies, source directional biasing was used by construction of a cumulative distribution function (cdf) based on a nonisotropic importance function. Conventional cylindrical coordinates  $(\rho, z, \phi)$  are used, where  $z$  is positive upward. If the particle direction cosine,  $x$ , is

$$x = z/(\rho^2 + z^2)^{1/2} ,$$

then the probability density function (pdf), which describes an isotropic source angular distribution, is

$$p(x) = 1/2, \quad -1 < x < 1 .$$

A suitable anisotropic pdf, which biases the selection toward certain target direction cosines  $x_i$ , is

$$p(x) = A \sum_{i=1}^N \left\{ 1 + \beta_i / [1 + \beta_i (x - x_i)^2] \right\} ,$$

where  $A$  normalizes  $p(x)$  to have an integral of unity (taken from  $x = -1$  to  $x = 1$ ) and where  $\beta_i$  and  $x_i$  are  $N$  bias strengths and bias directions. If a  $\beta_i$  is zero, there is no bias toward the corresponding  $x_i$ ; if all  $\beta_i$  are zero, the pdf is isotropic. The associated cdf is

$$c(x) = \int_{-1}^x p(x') dx' .$$

and the scattering direction is obtained in the usual way by selecting a random number,  $\xi$ , from the uniform distribution on  $(0,1)$  and then solving

$$c(x) = \xi$$

for  $x$ . The associated weight is simply  $1/p(x)$ .

The transport to the first collision was included as part of the source biasing and treated separately from subsequent transport biasing. In addition to the directional biasing already described, two types of path length biasing were used: (1) the well-known exponential transform and (2) an importance function. The exponential transform is not described further since it is a standard technique. For the importance function, instead of sampling from a simple exponential distribution,  $e^{-\alpha r}$ , in the transport integral

$$\int S e^{-\alpha r} dp ,$$

where  $\alpha$  is the range attenuation coefficient, we wish to sample from the distribution

$$(1 + \gamma r) e^{-\eta r} ,$$

where  $\gamma$  is an additional parameter and  $\eta$  is a different attenuation coefficient. Typically,  $\eta$  may be an order of magnitude smaller than  $\alpha$  to achieve deep penetration by the first scatter, and  $\gamma$  may be about unity. If  $\gamma$  is zero, the importance function reduces to the exponential transform, while if  $\gamma$  is about unity, the deep penetration statistics are markedly improved over the simple exponential transform. Since gamma ray buildup factors are roughly proportional to  $r$ , the  $\gamma r$  factor actually suffices to compensate for  $1/r^2$  geometric attenuation. A rejection method also was used to eliminate escapes before the first collision.

### 2.2.2 Transport Biasing

Several methods of biasing the transport kernel were used. A directional exponential transform was sometimes used to force longer transports in the outer direction, but was found unnecessary when region weight balancing and region importances were used with splitting and roulette.

Weight balancing involved keeping the particle weights near an optimum weight, which was a function of the distance from the burst. As necessary, particle weights were adjusted after each collision by splitting or playing roulette. Keeping the weights nearly the same within a volume detector caused the mean square weight to be close to the mean weight, leading to improved statistics. The optimum weight was the first collision weight multiplied by the approximate buildup factor,

$$w_{opt} = B(r) w_1(r) ,$$

where  $B(r)$  is the approximate buildup factor at range  $r$  from the burst and  $w_1(r)$  is the first-collision weight at range  $r$ . If no source transport bias were used, weight  $w_1(r)$  of a particle undergoing a first

collision at range  $r$  would be unity for all  $r$ . However, the use of the importance function described in section 2.2.1 causes weight  $w_1$  to be a function of  $r$ .

Region importances also were implemented. Various regions were assigned numerical ratings of their importance by the input to the SLEDGE code. For example, detectors near the ground were more important than detectors far above the ground. When a particle passed from a region of less importance to a region of greater importance, it was split. When passing the other way, roulette was played. Thus, more particles were tracked in more important regions, and fewer were tracked in less important regions.

### 2.2.3 Collision Biasing

In several problems, it was found helpful to use collision biasing, in which the emergent particle direction (scattering direction) was biased toward one or more areas of particular interest. The scattering direction was biased only for Compton scattering. For photo-absorption, the gamma ray is completely absorbed. For pair production, the scattering directions of the two locally produced annihilation quanta were assumed to be isotropic and opposite to each other. For Compton scattering, the bias importance function used was

$$I_C = \sum_{i=1}^M 1/[1 - \kappa_i(\hat{r} \cdot \hat{r}_i)] ,$$

where

$\kappa_i$  is the bias strength in the  $i$ th bias direction,  
 $\hat{r}$  is the unit vector in the scattering direction,  
 $\hat{r}_i$  is the unit vector in the  $i$ th bias direction.

The dot product  $\hat{r} \cdot \hat{r}_i$  is the cosine of the angle between  $\hat{r}$  and  $\hat{r}_i$  so that  $I_C$  is maximized when  $\hat{r}$  and  $\hat{r}_i$  are parallel.

Construction of a properly normalized pdf based on importance function  $I_C$  can be awkward, because the complete angular integral,

$$Q = \int_{4\pi} d\Omega I_C \sigma_C(\phi, \theta) ,$$

is required, where  $\sigma_C(\phi, \theta)$  is the Compton differential scattering cross section. Since  $\sigma_C(\phi, \theta)$  is not a simple function, the integral cannot be obtained analytically. A numerical integration would be time-consuming. Even a straightforward rejection method requires the same

integral to conserve particle weight. Hence, a special algorithm was devised to allow use of the rejection method to implement  $I_c$ . The algorithm uses recursive binary splitting with roulette to obtain exactly one surviving particle. The algorithm conserves weight and has a low variance. Briefly, the algorithm consists of the following steps to obtain the biased scattering direction,  $\Omega$ , for a particle of weight,  $W$ :

- (1) Select roulette variable  $V$  uniformly from the set (1,2).
- (2) Generate random trial scattering direction  $\Omega_1$  for a first split and get rejection probability  $R_1$ .
- (3) Test for rejection of the first split. If it is rejected, set  $W = W/2$  and return to step (2).
- (4) Otherwise, generate random trial scattering direction  $\Omega_2$  for a second split and get rejection probability  $R_2$ .
- (5) Test for rejection of the second split. If it is rejected, set  $W = W/(2 - 2/R_1)$ , set  $\Omega = \Omega_1$ , and go to Finish.
- (6) Otherwise, if  $V = 1$ , set  $W = W/(1 - R_1)$ , set  $\Omega = \Omega_1$ , and go to Finish.
- (7) Otherwise, if  $V = 2$ , set  $W = W/(1 - R_2)$ , set  $\Omega = \Omega_2$ , and go to Finish.

Finish This is the end of the algorithm.

This algorithm allows the use of the rejection method without the need to evaluate normalization integral  $Q$ .

In a number of SLEDGE runs, this algorithm was successfully used to push particles away from the ground and toward certain volume detectors with poor statistics.

### 2.3 Cross Sections

The well-known Klein-Nishina expressions were used for the Compton scattering cross section. For the media under consideration (air and ground), the Compton cross section dominates cross sections for photoabsorption and pair production over a wide energy range.

The attenuation coefficient for pair production was approximated by the simple expression

$$\tau_{pp} = 1.84 \times 10^{-4} \rho \bar{Z}^2 (\hat{E} - 0.014\hat{E}^2) / \bar{A},$$

where

$\tau_{pp}$  is in inverse centimeters,

$\rho$  is the material density in grams per cubic centimeter,

$\bar{Z}^2$  is the mean square atomic number of the material,

$\hat{E}$  is  $E - 1.022$ , and  $E$  is the gamma ray energy in MeV,

$\bar{A}$  is the mean atomic weight of the material.

For air,  $\bar{Z}^2 = 106.4$  and  $\bar{A} = 28.9$ .

For aluminum,  $\bar{Z}^2 = 13^2$  and  $\bar{A} = 27.0$ .

The attenuation coefficient for photoabsorption was approximated by

$$\tau_{ph} = \frac{1.88 \times 10^{-2} \rho \bar{Z}^4}{\bar{A} (100E)^{3.49 - 0.0035 (\log \bar{Z}^4)^2}}$$

where the logarithm is to the base 10. The material mean fourth power of the atomic number is  $6.46 \times 10^3$  for air and  $13^4$  for aluminum. This approximation has no significant error for air, but is about 10 percent low for aluminum.

The error incurred in the total absorption cross section by using these approximations appears to be less than 1 percent in air for gamma ray energies from 0.01 to 10 MeV. The error in aluminum is slightly greater for energies less than 0.1 MeV. The values for aluminum are cited here because the air-over-ground transport studies were done over an aluminum ground for simplicity. The gamma ray cross-section properties of aluminum are similar to a typical ground composed of silicon, aluminum, oxygen, and water.

#### 2.4 Scoring EMP Drivers by Correlated Sampling

A particularly useful innovation in the SLEDGE code concerns exploitation of the correlation between the energy deposition response function and the (Compton and photoelectric) electron current response function. When EMP drivers are scored, the electron current contribution is found to be correlated with the associated energy deposition contribution. The correlation is high at early times when the gamma ray direction is well collimated, but becomes low at later times when the gamma ray direction is poorly collimated. Ultimately, the correlation drops to zero as the many scatters produce an isotropic gamma direction. The correlation can be exploited in the following way.

Define the energy deposition score in a volume detector,  $k$ , and time bin,  $l$ ,

$$S_{kl} = \frac{1}{n} \sum_{m=1}^n s_{klm}$$

and the radial (for example) electron current as

$$J_{kl} = \frac{1}{n} \sum_{m=1}^n j_{klm}$$

where  $m$  denotes the batch number of a total of  $n$  batches. Thus,  $s_{klm}$  is the energy deposition score for the  $k$ th detector,  $l$ th time bin, and  $m$ th batch. Define also arbitrary function  $H_{kl}$ , which depends on the detector and the time bin. Consider the variance of the linear combination  $J_{kl} - H_{kl}S_{kl}$ :

$$\text{VAR} \{J_{kl} - H_{kl}S_{kl}\} = \sum_m j_{klm}^2 - 2H_{kl} \sum_m j_{klm}s_{klm} + H_{kl}^2 \sum_m s_{klm}^2$$

If  $j_{klm}$  and  $H_{kl}s_{klm}$  are positively correlated, the negative term on the right hand side reduces the variance; if the correlation coefficient of  $j_{klm}$  and  $H_{kl}s_{klm}$  is unity, the right hand side becomes zero. Therefore, on the assumption that  $j_{klm}$  and  $H_{kl}s_{klm}$  are at least partly correlated, solve the equation

$$j_{klm} = H_{kl}s_{klm}$$

for  $H_{kl}$  by least-squares regression. This regression value for  $H_{kl}$  should minimize

$$\text{VAR} \{J_{kl} - H_{kl}S_{kl}\}$$

and make optimum use of any correlation between  $j_{klm}$  and  $H_{kl}s_{klm}$ .

In practice with the SLEDGE code, this correlated sampling technique improved the electron radial current fractional deviation statistics by more than an order of magnitude, except at later times when all remaining gamma rays have been scattered many times. The electron theta current statistics were similarly improved by more than a factor of two, especially at late times when significant theta currents were developing.

### 3. CALCULATIONS PERFORMED

#### 3.1 One-Dimensional Studies

The principal aspects of gamma ray transport can be described in terms of buildup factors. (A buildup factor for an effect is the ratio of the effect as engendered by uncollided and multiply scattered gamma ray flux, to the effect as engendered by uncollided gamma flux.) The SLEDGE code was run for seven discrete gamma ray energy sources (table 1) in a homogeneous free air geometry. Results for the time integrated energy deposition buildup factor were obtained from 25 1-d radial bins, each 1 attenuation length wide, extending to a maximum range of 25 attenuation lengths. Fractional deviations varied from about 3 percent at the closer radial bins to about 10 percent for the most distant. For each gamma ray energy, a SLEDGE run was made consisting of 25 batches of 4000 histories each, for a total of 100,000 histories. A typical run tallied about one million collisions (scatters) and consumed about 40 min of central processing unit (CPU) time on the HDL computer (an IBM 370/168). Results were stored on magnetic tape for subsequent analysis and curve fitting.

TABLE 1. SEVEN GAMMA RAY ENERGIES AND ATTENUATION PARAMETERS

Source gamma ray energy (MeV)	Total attenuation coefficient ( $m^{-1}$ )	1 attenuation length (m)	25 attenuation lengths (m)
0.5	0.009604	104.12	2603.08
1.0	0.007014	142.57	3564.30
1.5	0.005734	174.40	4359.96
2.5	0.004377	228.47	5711.67
3.5	0.003651	273.90	6847.44
5.0	0.003034	329.60	8239.95
7.0	0.002596	385.21	9630.20

Table 1 lists the total attenuation coefficient and distances corresponding to 1 and 25 attenuation lengths. An air density of  $1.11 \times kg/m^3$  is assumed.

Time-dependent results also were obtained from these studies. The time bin structure used was the same as for the 2-d problems, shown in table 2.

TABLE 2. SLEDGE MESHES FOR TWO-DIMENSIONAL PROBLEMS

Time bin boundaries (s)	Radial boundaries (m)	Vertical boundaries (m)
0.00	0.0	-1.0
5.00(-9) <sup>a</sup>	300.0	0.0 <sup>b</sup>
1.00(-8)	600.0	25.0
2.00(-8)	900.0	50.0
3.25(-8)	1200.0	100.0
5.00(-8)	1500.0	200.0
7.50(-8)	1800.0	400.0
1.00(-7)	2100.0	600.0
1.50(-7)	2400.0	3000.0
2.00(-7)	2700.0	
3.00(-7)	3000.0	
4.00(-7)		
6.00(-7)		
1.00(-6)		
1.50(-6)		
2.00(-6)		
3.00(-6)		
5.00(-6)		
1.00(-5)		

<sup>a</sup>Read as  $5.00 \times 10^{-9}$ .

<sup>b</sup>Air-ground interface at 0.0-m height.

### 3.2 Two-Dimensional Air-Ground Interface Effects

The 2-d air-over-ground gamma ray transport problem may be considered as a perturbed free-field problem. Significant perturbations are expected near the air-ground interface. The SLEDGE code was run for a 1.5-MeV gamma ray source in a cylindrical air-over-ground geometry. A burst height of 200 m was used. As mentioned in section 2.3, the ground was assumed for simplicity to be aluminum, whose gamma ray cross-section

properties are analogous to a typical ground composed of silicon, aluminum, oxygen, and water. The radial (horizontal) mesh extended to a 3000-m ground range, and the vertical mesh extended to a 3000-m height aboveground and to a 1-m depth belowground. Eighteen time bins were used, extending to a 10- $\mu$ s retarded time. These grids are shown in table 2. Correlated sampling was used for the radial Compton current, but not for the theta Compton current. Various biases and importance functions were used, as described in section 2.2. The run consisted of 30 batches of 20,000 histories each, for a total of 600,000 histories. In longer than 2 hr of CPU running, nearly four million collisions (scatters) were tallied. Fractional deviations for energy deposition averaged 1 percent close to the burst and about 6 percent near the 3-km boundary.

It was observed that energy deposition from outgoing gamma rays was about eight times that from backscattered incoming gamma rays, at any range in the air. The backscatter from the ground was much less, so that radial Compton current and energy deposition were weaker near the ground and the theta Compton current was strongest. This effect is clear since gamma rays must flow from the air into the ground and be attenuated there; this flow causes a negative gradient in the flux close to the ground. From a different viewpoint, the buildup factor is reduced near the ground.

Since effects due to multiply scattered gamma rays come later in time than effects due to unscattered gamma rays, the time dependence of effects was confirmed to be range dependent. At deeper penetrations, the buildup factor is greater so that multiply scattered effects are stronger. The result is that the energy deposition decay rate in time is slower at deeper penetrations. The ratio of radial Compton current to energy deposition rate also declines with time more slowly with increasing range. In fact, the time dependence of the latter ratio roughly scales as the inverse of the buildup factor (that is, scaled time  $t' = tB$ ).

A similar SLEDGE run was done for a 0.5-MeV gamma ray source. Results of both runs were stored on magnetic tape for subsequent analysis.

## PART II. ANALYTICAL FITS TO EMP DRIVER RESULTS

### 4. ENERGY DEPOSITION

#### 4.1 Fitting Free-Field Buildup Factors for Seven Gamma Ray Energies

Seven gamma ray energies from 0.5 to 7.0 MeV (table 1) were chosen to allow flexibility in representing approximately an arbitrary nuclear burst gamma ray energy spectrum. Since gamma-induced EMP sources may contribute to EMP generation at distances as great as about 5 km, the gamma ray transport was carried to a range of 25 attenuation lengths to ascertain the true range dependence of the buildup factor for energy deposition. Based on theory, a reasonable approximation to the buildup factor is given by

$$B(r) = 1 + a(r/\lambda)^k ,$$

where  $\lambda$  is the attenuation length and  $a$  may be shown by energy conservation to be

$$a = \mu_s / [\mu_a \Gamma(k+1)] ,$$

where

$\mu_s$  = total scattering coefficient ( $\mu_s = \sigma_s + 1.022\sigma_{pp}/E$ ),

$\sigma_s$  = Compton scattering coefficient,

$\sigma_{pp}$  = pair production attenuation coefficient,

$E$  = gamma ray energy in MeV,

$\mu_a$  = total absorption coefficient for Compton absorption, photoabsorption, and pair production  
[ $\mu_a = \sigma_a + \sigma_{ph} + \sigma_{pp}(E - 1.022)/E$ ] ,

$\sigma_a$  = Compton absorption coefficient,

$\sigma_{ph}$  = photoabsorption attenuation coefficient,

$\Gamma(k+1)$  = gamma function of  $k+1$ ,

$k$  = function of (source) gamma ray energy.

Parameter  $k$  is of order unity and is the only free quantity in the expression for  $B$ .

The expression for  $B$  was fitted, by adjustment of  $k$ , to the 1-d detector results obtained by the SLEDGE code. Twenty-five detectors were used, each one attenuation length thick. The least-squares fit was

obtained by minimizing the sum of the squares of the errors over all detectors, with each square weighted by the reciprocal of the square of the fractional deviation for the detector. Buildup factor parameters  $a$  and  $k$  so obtained are given in table 3 for each gamma ray energy. The buildup factor predicted by these values of  $a$  and  $k$  has a probable error of not more than 1 percent due to the uncertainty in the Monte Carlo data. Although the fractional deviation for the detectors varies from about 3 to about 10 percent, the combined fractional deviation (of all 25 detectors fitted at once) is less than 1 percent. However, this 1-percent error estimate does not include the possibility of systematic error due to the true buildup factor not being perfectly represented by the expression  $1 + a(r/\lambda)^k$ . This error estimate does describe how closely the  $a$  and  $k$  parameter values, thus obtained by fitting Monte Carlo data, approximate the best fit of the expression to the true buildup factor.

As to possible systematic error, it appears that the fit may be low by about an average 2 percent to 10 attenuation lengths range, but this level remains uncertain because of the size of statistical error of the Monte Carlo data. Statistical error at farther ranges is even greater and permits no assessment of systematic error.

TABLE 3. ENERGY DEPOSITION BUILDUP FACTOR PARAMETERS FOR  $B = 1 + a(r/\lambda)^k$

Source gamma ray energy (MeV)	a	k
0.5	1.534	1.418
1.0	1.162	1.188
1.5	0.960	1.143
2.5	0.800	0.976
3.5	0.695	0.903
5.0	0.580	0.880
7.0	0.473	0.891

#### 4.2 Ground Effect on Buildup Factor

Analysis of the 2-d detector results of the two SLEDGE runs, for 0.5- and 1.5-MeV gamma ray point sources at 200 m aboveground, showed a distinct depletion of energy deposition near the ground. An exception is that early energy deposition is enhanced beneath the burst due to immediate backscatter from the ground. However, this effect will be neglected in the following development since EMP in this region is not important to typical Army electronic systems because of overwhelming blast and thermal damage.

For observers near the ground and for a range such that the line of sight to the burst is shallow, the buildup factor was limited in its growth. This limitation was interpreted that the ground (although

flat) introduced an effective horizon because the ground intercepts multiply scattered gamma rays that would otherwise contribute. The effective horizon,  $H$ , is approximately

$$H = 3.0r / (9.0 + r^2/\lambda^2)^{1/2}$$

for horizontal gamma ray incidence near the ground.

The effective horizon for horizontal incidence,  $h$ , at height  $z$  aboveground is approximately

$$h = H e^{z/\lambda} .$$

For incidence at angle  $\theta$  to the horizontal, the effective horizon at the observer will be approximated by the averaging integral

$$h = \int_0^H e^{z(r)/\lambda} dr = \int_0^H e^{[r(\sin\theta)+Z]/\lambda} dr ,$$

or

$$h = \frac{\lambda e^{Z/\lambda}}{\sin \theta} \left[ e^{H(\sin\theta)/\lambda} - 1 \right] ,$$

where  $z(r)$  is the height at range  $r$  on the line of sight from the burst to the observer and  $Z$  is the observer height aboveground.

The ground-influenced buildup factor,  $\hat{B}(R,Z)$ , a function of observer range and height, is asymptotically limited to  $B(h)$ , that attained within effective horizon  $h$ . Based on the SLEDGE 2-d results, a good approximation for the ground-influenced buildup factor is

$$\hat{B}(R,Z) = (1/2)[B(r) + X] ,$$

where  $B(r)$  is the free-field buildup factor for range  $r$  from the source and

$$X = 1 + 1 / \left\{ 1/[B(r) - 1]^2 + 1/[4 + [B(h) - 1]^2] \right\}^{1/2} .$$

#### 4.3 Time Dependence of Energy Deposition Rate

The time-dependent energy deposition rate,  $S$ , at distance  $r$ , height  $z$ , and time  $t$  contributed by multiply scattered gamma rays (that is, excluding uncollided gamma rays) from a delta-function (in time) point gamma source of one gamma of energy,  $E$ , is written as

$$S(r,z,t) = U(r)N(r,z)T(r,z,t) ,$$

where

$U(r)$  = energy deposition from uncollided gamma ray number flux (that is, first-scatter deposition),

$N(r,z)$  = normalization factor (including buildup factor),

$T(r,z,t)$  = explicit time dependence.

$U(r)$  is given by

$$U(r) = Ee^{-r/\lambda} / (4\pi r^2 \lambda_{\text{abs}}) ,$$

where  $E$  is the gamma ray energy,  $\lambda$  is the attenuation length, and  $\lambda_{\text{abs}}$  is the absorption length. Based on the 1.5-MeV gamma ray source SLEDGE results, a good approximation for  $T$  is

$$T(r,z,t) = (t + t_0)^m e^{-pt} ,$$

where

$$t_0 = 10^8 \text{ s} ,$$

$$m = -1/[1 + f(r,z)r/\lambda] ,$$

$$p = 1.4 \times 10^6 \text{ s}^{-1} .$$

Function  $f(r,z)$  is described later.

We require  $S$  to be independent of  $z$  at  $t = 0$  since the ground affects only multiply scattered gamma rays (for an observer above-ground), and these gamma rays always arrive after  $t = 0$ . We require also the following normalization:

$$\int_0^{\infty} S(r,z,t) dt = U(r) [\hat{B}(r,z) - 1] ,$$

where  $\hat{B}$  is the ground-influenced buildup factor. For  $z = \infty$ ,  $\hat{B}$  becomes free-field buildup factor  $B(r)$ . From this normalization, we obtain

$$N(r,z) \int_0^{\infty} T(r,z,t) dt = \hat{B}(r,z) - 1 .$$

Let  $I$  be defined as the integral

$$\begin{aligned} I &= \int_0^{\infty} T(r,z,t) dt \\ &= \int_0^{\infty} (t + t_0)^m e^{-pt} dt . \end{aligned}$$

By straightforward means, the integral is found to be

$$I = e^{pt_0} p^{-\epsilon} \Gamma(\epsilon) [1 - P(\epsilon, pt_0)] ,$$

where

$$\epsilon = 1 + m ,$$

$$\Gamma(\epsilon) = \text{gamma function of } \epsilon ,$$

$$P(\epsilon, pt_0) = \text{incomplete gamma function.}^5$$

Hence, normalization factor  $N(r, z)$  is

$$N(r, z) = [\hat{B}(r, z) - 1] / I .$$

Since function  $f(r, z)$  has not been specified yet, variable  $\epsilon$ ,

$$\epsilon = 1 - 1/[1 + f(r, z)r/\lambda] ,$$

remains unconstrained. We use it to satisfy the requirement that  $S(r, z, t)$  be independent of  $z$  at  $t = 0$ . At earliest times, the transport is essentially free field, so free-field data far from the ground should describe the  $t = 0$  transport. By examination of SLEDGE data for detectors far from the ground (virtually free field), it was determined that a value  $f = 0.2$  would cause  $S$  to fit these data reasonably well. This value is called  $f_\infty$  (that is,  $f_\infty \cong 0.2$ ). Let the corresponding value for  $\epsilon$  be

$$\epsilon_\infty = 1 - 1/(1 + f_\infty r/\lambda) .$$

We require the transport near the ground at  $t = 0$ , to be the same as the transport far ( $z \rightarrow \infty$ ) from the ground, also at  $t = 0$ . Thus,

$$S(r, z=\infty, t=0) \cong S(r, z, t=0) ,$$

or

$$\frac{[B(r) - 1]T(r, z=\infty, t=0)}{I(r, z=\infty)} = \frac{[\hat{B}(r, z) - 1]T(r, z, t=0)}{I(r, z)} .$$

This can be expanded to

$$\frac{[B(r) - 1]t_0^{\epsilon_\infty - 1}}{e^{pt_0} p^{-\epsilon_\infty} \Gamma(\epsilon_\infty) [1 - P(\epsilon_\infty, pt_0)]} = \frac{[\hat{B}(r, z) - 1]t_0^{\epsilon - 1}}{e^{pt_0} p^{-\epsilon} \Gamma(\epsilon) [1 - P(\epsilon, pt_0)]} ,$$

<sup>5</sup>Milton Abramowitz and Irene Stegun, *Handbook of Mathematical Functions*, Dover Publications, Inc., New York (1965), 260.

where  $\epsilon$  is a function of  $z$ . If we define  $G(\epsilon)$  by

$$G(\epsilon) = t_0^{1-\epsilon} e^{pt_0} p^{-\epsilon} \Gamma(\epsilon) [1 - P(\epsilon, pt_0)] ,$$

then this may be written

$$[B(r) - 1]/G(\epsilon_\infty) = [\hat{B}(r, z) - 1]/G(\epsilon) ,$$

or

$$G(\epsilon) = G(\epsilon_\infty) [\hat{B}(r, z) - 1] / [B(r) - 1] .$$

Thus, given  $r$  and  $z$ ,  $G(\epsilon)$  may be determined from  $G(\epsilon_\infty)$ ,  $B(r)$ , and  $\hat{B}(r, z)$ .  $G(\epsilon)$  may then be inverted to yield  $\epsilon$ . Having  $\epsilon$  and  $m = \epsilon - 1$ , one may obtain

$$\begin{aligned} I &= G(\epsilon) t_0^m , \\ N(r, z) &= [\hat{B}(r, z) - 1] / I , \\ T(r, z, t) &= (t + t_0)^m e^{-pt} , \\ S(r, z, t) &= U(r) N(r, z) T(r, z, t) . \end{aligned}$$

Inverting  $G(\epsilon)$  for  $\epsilon$  involves tabulating  $G$  for a large number of values of  $\epsilon$  and then using a table-lookup algorithm to get  $\epsilon$  from  $G$ .

By using the approach just described, the energy deposition rate may be obtained for any  $r, z, t$  in such a way that it evolves in time from an initial free-field distribution to a progressively more ground-influenced distribution. Time integrals of the energy deposition rate are correctly normalized to expected ground-influenced buildup factors.

These results are scaled to first order to source gamma ray energies other than 1.5 MeV by geometrically scaling  $r$ ,  $z$ , and  $t$  by the attenuation length. This is already built into buildup factors  $B$  and  $\hat{B}$  and variable  $m$  (and  $\epsilon$ ). Only the time remains to be scaled. If subscript "1.5" denotes 1.5-MeV source gamma rays and if

$$\alpha \equiv \lambda_{1.5} / \lambda(E) ,$$

where  $\lambda(E)$  is the attenuation length for gamma ray energy  $E$ , then

$$G(\epsilon) = (\alpha t_0)^{1-\epsilon} e^{\alpha p \alpha t_0} p^{-\epsilon} \Gamma(\epsilon) [1 - P(\epsilon, \alpha p \alpha t_0)] ,$$

$$I = G(\epsilon) (\alpha t_0)^m / \alpha ,$$

$$T(r, z, t) = (\alpha t + \alpha t_0)^m e^{-\alpha p \alpha t} .$$

Variable  $m$  is evaluated for  $\lambda = \lambda(E)$  as

$$m = - 1/[1 + fr/\lambda(E)] .$$

The uncollided energy deposition,  $U$ , becomes

$$U(r) = Ee^{-r/\lambda(E)}/[4\pi r^2 \lambda_{\text{abs}}(E)] .$$

## 5. RELATION OF COMPTON CURRENT TO ENERGY DEPOSITION RATE

### 5.1 Compton Current from First Collisions of Gamma Rays

For point source gamma rays experiencing their first collision in air having density  $1.11 \text{ kg/m}^3$ , the radial Compton current produced is simply related to the corresponding energy deposition:

$$J_r/S = k_0(E) .$$

The theta Compton current,  $J_\theta$ , is identically zero for first scatters. Factor  $k_0(E)$  is given in table 4 for the seven gamma ray energies considered. The values are based on estimates<sup>6</sup> of the mean forward range of Compton electrons, including multiple scattering of the Compton electrons as well. Factor  $k_0(E)$  equals  $\lambda_a R_c / (\rho \lambda_c E)$ , where  $\lambda_a$  and  $\lambda_c$  are the Compton absorption and collision lengths,  $\rho$  is the air density,  $R_c$  is the mean forward range of the Compton electrons, and  $E$  is the gamma ray energy.

TABLE 4. RATIO OF RADIAL COMPTON ELECTRON CURRENT TO ENERGY DEPOSITION FOR FIRST-COLLISION GAMMA RAYS FROM A POINT SOURCE

Source gamma ray energy (MeV)	Ratio $k_0(E)$ (electron-cm/MeV)
0.5	1.061
1.0	1.606
1.5	1.952
2.5	2.338
3.5	2.508
5.0	2.561
7.0	2.454

<sup>6</sup>William T. Wyatt, Jr., *Transmission Factor Effects on the Average Forward Range of Compton Electrons*, Harry Diamond Laboratories HDL-TM-80-10 (January 1980).

## 5.2 Radial Compton Current from Multiply Scattered Gamma Rays

For multiply scattered gamma rays, the radial Compton current produced is related to the corresponding energy deposition by

$$J_r/S = k(r,t,E) ,$$

where  $r$  is the distance from the point source of gamma rays and  $t$  is retarded time. The SLEDGE 1-d results for each of the seven gamma ray energies can be fitted by

$$k(r,t,E) \approx k_0(E)(0.91 + 0.03E^{1/2})e^{-T} ,$$

where

$$T = \frac{1.0 \times 10^{-8} p_1 (1.0 \times 10^8 t)^{p_2}}{[B(R) - 1]^{p_4}}$$

and

$$R = r + \lambda(p_3 + p_5 t/[r/\lambda]^{p_6}) .$$

Factor  $k_0(E)$  is defined in section 5.1. Buildup factor  $B$  is evaluated for modified range  $R$ . Optimum fit values for  $p_1, p_2, p_3, p_4, p_5,$  and  $p_6$  are listed in table 5 for the seven gamma ray energies.

TABLE 5. FIT PARAMETERS FOR RATIO OF RADIAL COMPTON ELECTRON CURRENT TO ENERGY DEPOSITION RATE FOR MULTIPLY SCATTERED GAMMA RAYS

Source gamma ray energy (MeV)	$p_1$	$p_2$	$p_3$	$p_4$	$p_5$	$p_6$
0.5	3.880(7) <sup>a</sup>	1.384	7.599(-2)	0.855	2.793(7)	-0.0847
1.0	1.783(7)	1.040	1.304(-1)	0.685	0.817(7)	+0.0524
1.5	1.162(7)	1.025	7.358(-2)	0.596	0.537(7)	-0.1179
2.5	0.964(7)	0.974	1.765(-2)	0.679	0.339(7)	+0.0605
3.5	0.769(7)	0.974	1.679(-2)	0.758	0.247(7)	+0.1410
5.0	0.358(7)	1.230	7.253(-2)	0.947	0.523(7)	-0.1091
7.0	0.835(6)	1.865	7.869(-2)	1.561	1.336(7)	-0.0886

<sup>a</sup>Read as  $3.880 \times 10^7$ .

Quantity  $k(r,t,E)$  decays more slowly with increasing range. Also, in theory one would expect  $k$  at time  $t = 0$  to be exactly  $k_0(E)$  since the earliest scattered gamma rays to arrive at any point are those that have experienced a single grazing scatter and thus have nearly the same energy,  $E$ . However, the Monte Carlo studies show that

$$k(r,t,E) \approx k_0(E)(0.91 + 0.03E^{1/2})$$

when averaged over the first time bin, which is 5 ns wide. This resolution of the time history appears to be adequate since most gamma ray output from a nuclear burst is emitted over about 10 ns.

### 5.3 Theta Compton Current from Multiply Scattered Gamma Rays

The theta Compton current from a point gamma ray source near the earth is secondary to the radial Compton current in magnitude and in efficiency as a generator of EMP. In the SLEDGE 2-d results, variance was larger for the theta current component--often so large that the sign of the component was doubtful. Nevertheless, some significant trends were clearly observed at late times near the ground. The ratio of theta Compton current to energy deposition rate (for an air density of  $1.11 \text{ kg/m}^3$ ) is approximately

$$J_\theta/S = 1.5 \times 10^5 t e^{-0.02z} ,$$

where  $t$  is retarded time in seconds and  $z$  is height aboveground in meters. Thus, the theta component is strongest near the ground and decays (about) exponentially with increasing height.

This expression for  $J_\theta/S$  is not strongly dependent upon source gamma ray energy to a first approximation since the late-time currents derive from low-energy multiply scattered gamma rays.

## 6. COMPARISON WITH PREVIOUS RESULTS

### 6.1 Buildup Factor for Energy Deposition

The LEMP code prompt gamma ray drivers (H. J. Longley, Mission Research Corp.) include buildup factor curve fits for energy deposition and radial Compton current for three source gamma ray energies (0.5, 1.5, and 5.0 MeV). No account is taken of the influence of the ground. The energy deposition buildup factor obtained for air was based on published data for water.

Recently, Malik, Cashwell, and Schrandt<sup>7</sup> at the Los Alamos Scientific Laboratory (LASL) obtained curve fits to buildup factors and

<sup>7</sup>J. S. Malik, E. D. Cashwell, and R. G. Schrandt, *The Time Dependence of the Compton Current and Energy Deposition from Scattered Gamma Rays*, Los Alamos Scientific Laboratory, NM, LA-7386-MS (July 1978).

time dependence of energy deposition and Compton current from scattered gamma rays in homogeneous isotropic air. These curve fits to their Monte Carlo data were obtained for gamma ray energies of 1, 1.5, 2, 3, 4, and 6 MeV to a range of 1600 m. Air density was  $1.1 \text{ mg/cm}^3$ .

The LEMP and LASL buildup factors are compared with NEMP free-field and ground-influenced buildup factors (for energy deposition) in figures 1 to 6. The NEMP ground-influenced buildup factor is for a burst and an observer both at a 0-m height aboveground. Figures 1 to 3 show results as a function of range in units of attenuation lengths, from 0 to 25 attenuation lengths. These results exclude the effect of any disagreement in attenuation length among the LEMP, LASL, and NEMP drivers and compare directly the functional forms used. Figures 1 to 3 show, respectively, 0.5-, 1.5-, and 5.0-MeV source gamma ray buildup factors. The 0.5-MeV energy is below the 1.0-MeV lower limit for the LASL transport data and shows that the LASL drivers are in substantial error below the designated range. The LEMP and NEMP curves are in good agreement to about four attenuation lengths range, after which the LEMP curve is higher. For 0.5 MeV, the disagreement becomes very large. The quality of agreement between LEMP and NEMP at closer ranges, however, tends to confirm their validity at such ranges. The LASL curves, on the other hand, seem too low except for the 5.0-MeV results (fig. 3). The low-energy disagreement among LEMP, NEMP, and LASL is ameliorated by the fact that, for a realistic gamma ray energy spectrum, higher energy gamma rays predominate at substantial ranges because of their greater penetrating ability.

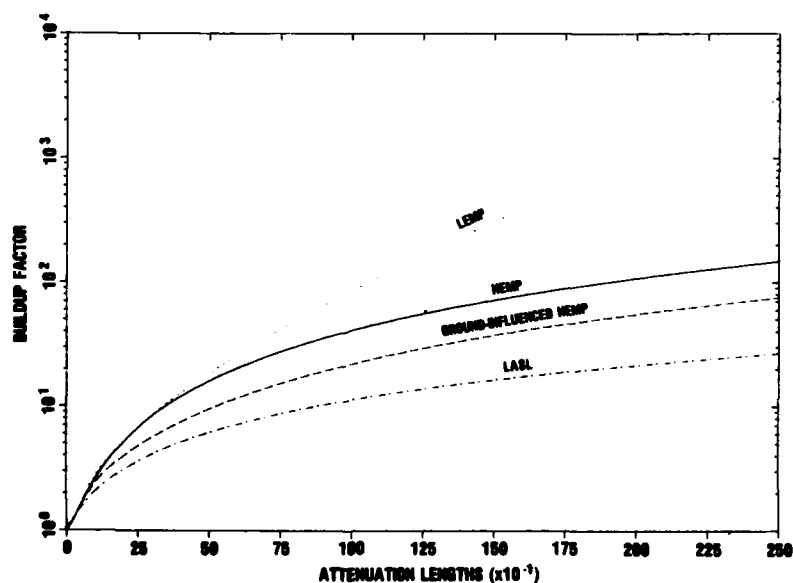


Figure 1. Energy deposition buildup factors compared for 0.5-MeV gamma rays, for range in attenuation lengths.

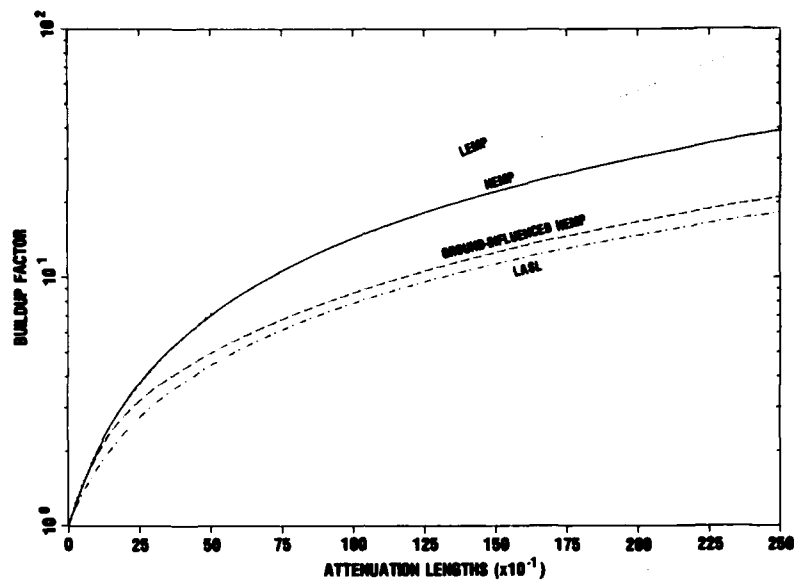


Figure 2. Energy deposition buildup factors compared for 1.5-MeV gamma rays, for range in attenuation lengths.

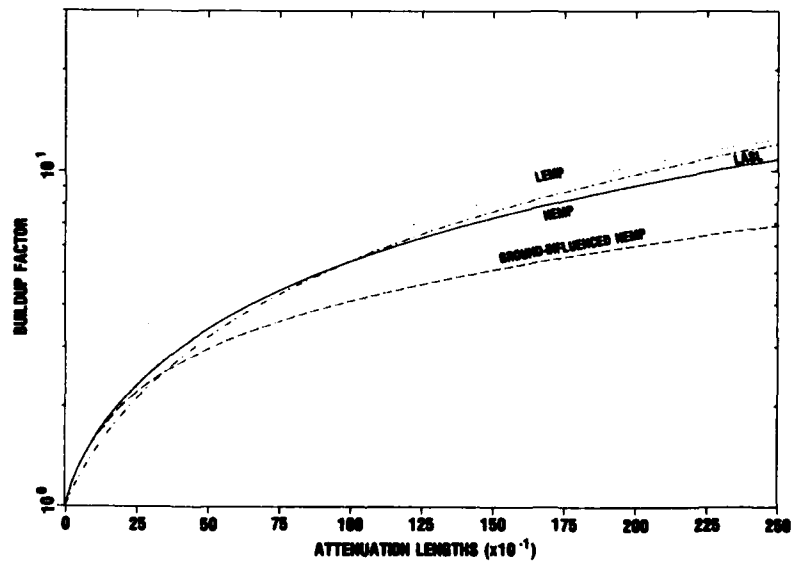


Figure 3. Energy deposition buildup factors compared for 5.0-MeV gamma rays, for range in attenuation lengths.

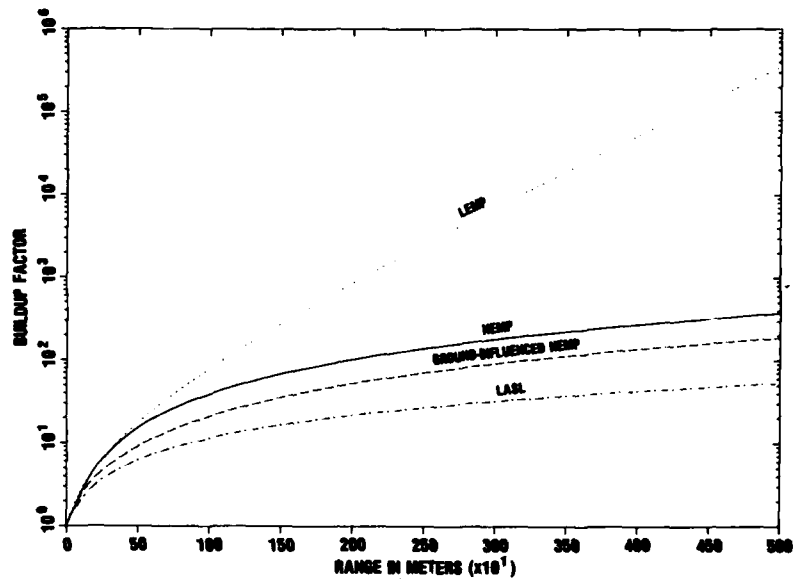


Figure 4. Energy deposition buildup factors compared for 0.5-MeV gamma rays, for range in meters.

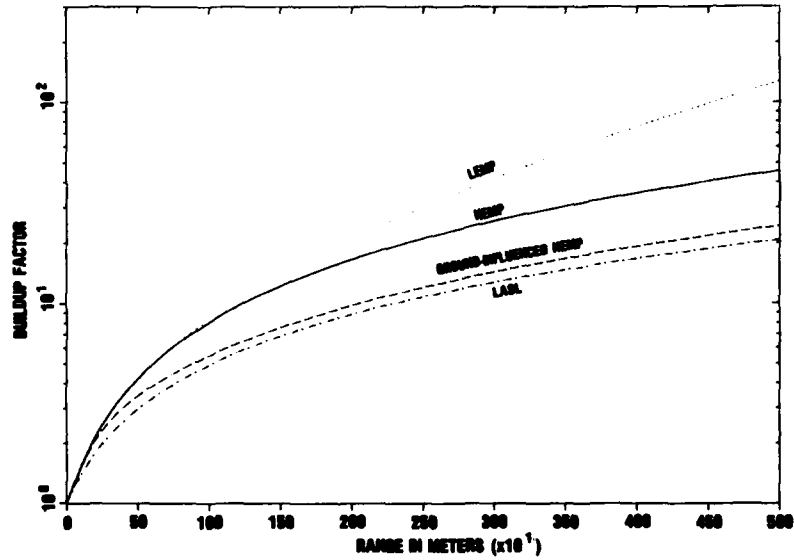


Figure 5. Energy deposition buildup factors compared for 1.5-MeV gamma rays, for range in meters.

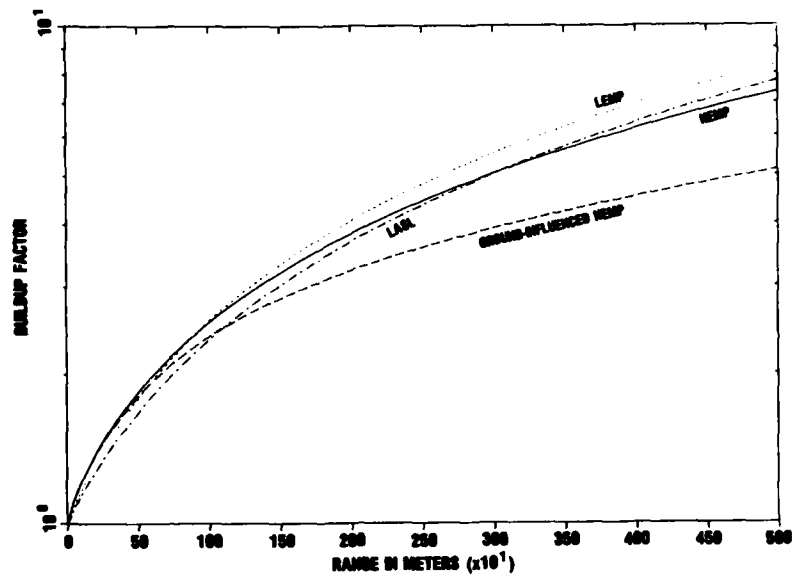


Figure 6. Energy deposition buildup factors compared for 5.0-MeV gamma rays, for range in meters.

Figures 4 to 6 include the attenuation length, but still appear similar to figures 1 to 3. Careful comparison of SLEDGE transport results with the NEMP curve fit shows that the NEMP curve fit is about 10 percent higher over the first attenuation length. But the NEMP curve fit is found to be accurate to a few percent at greater ranges.

The NEMP ground-influenced buildup factor in figures 1 to 6 is as much a factor of two smaller than the corresponding NEMP free-field buildup factor. The difference increases monotonically with range, more slowly for more energetic gamma rays, to a difference of as much as a factor of two.

## 6.2 Time Dependence of Energy Deposition Rate

The time dependence of the free-field NEMP, LEMP, and LASL energy deposition rate drivers is shown in figures 7 to 12 for three source gamma ray energies (0.5, 1.5, and 5.0 MeV) and two ranges from the burst (300 and 3000 m). The three curves are normalized to a time integral of unity, removing any disagreement in attenuation length and buildup factor. A fourth curve represents the ground-influenced NEMP energy deposition rate for burst and observer on the ground. This curve is normalized to the free-field case, so the difference between this curve and the free-field NEMP curve is a diminution of the energy deposition rate due to the presence of the ground.

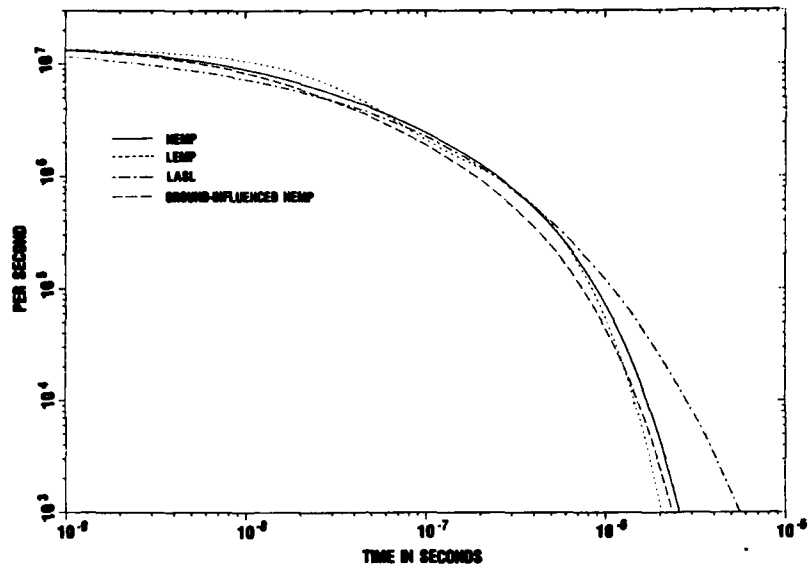


Figure 7. Time dependence of energy deposition buildup factors compared at 300-m range for 0.5-MeV gamma rays.

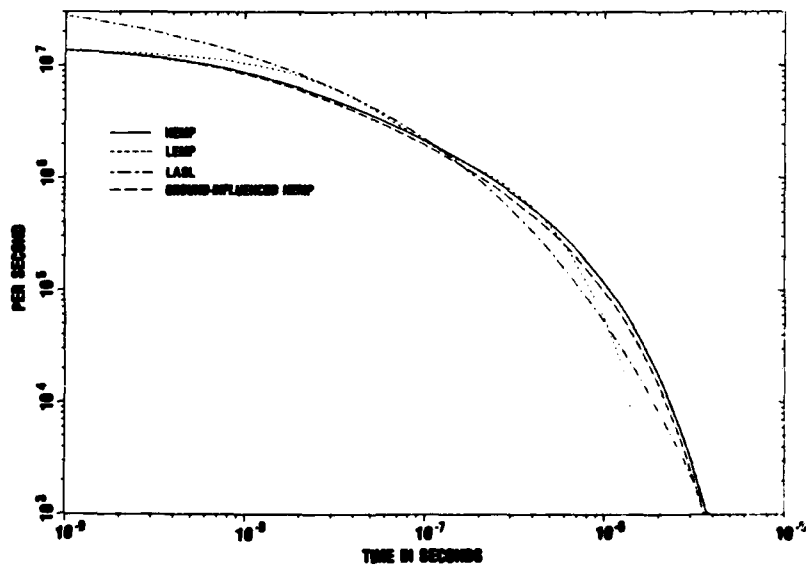


Figure 8. Time dependence of energy deposition buildup factors compared at 300-m range for 1.5-MeV gamma rays.

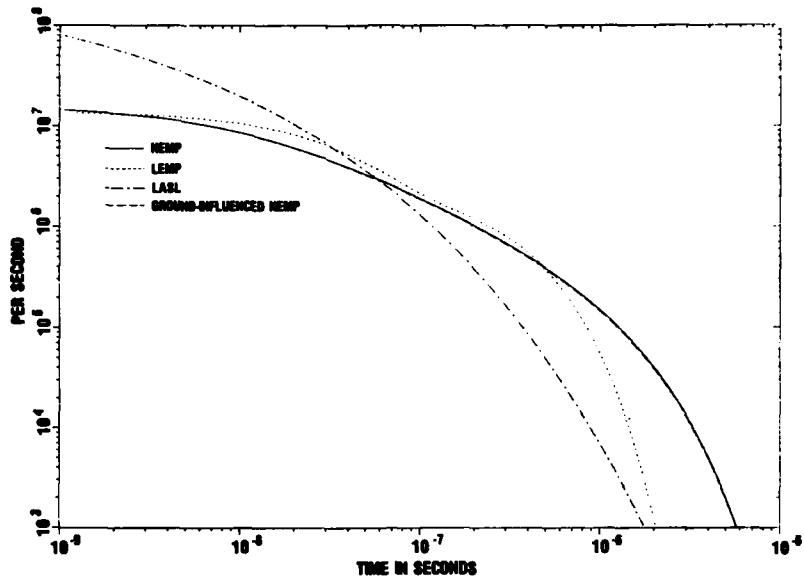


Figure 9. Time dependence of energy deposition buildup factors compared at 300-m range for 5.0-MeV gamma rays.

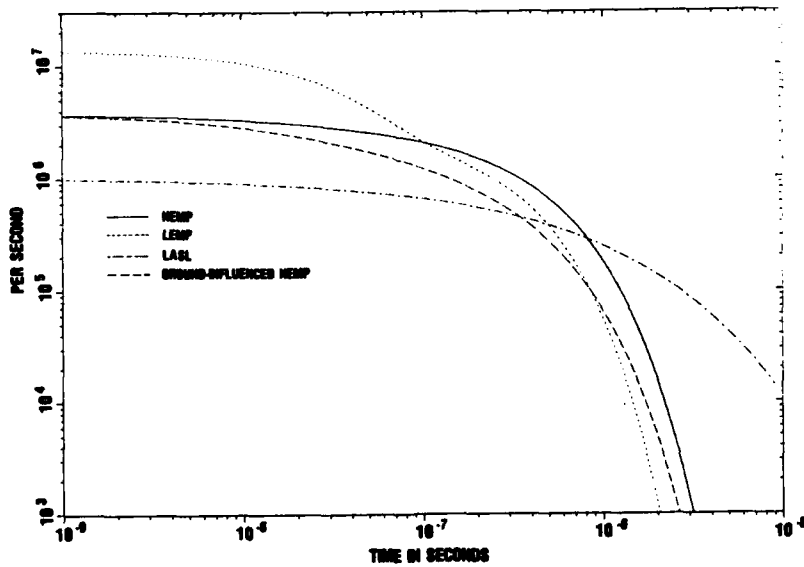


Figure 10. Time dependence of energy deposition buildup factors compared at 3000-m range for 0.5 MeV-gamma rays.

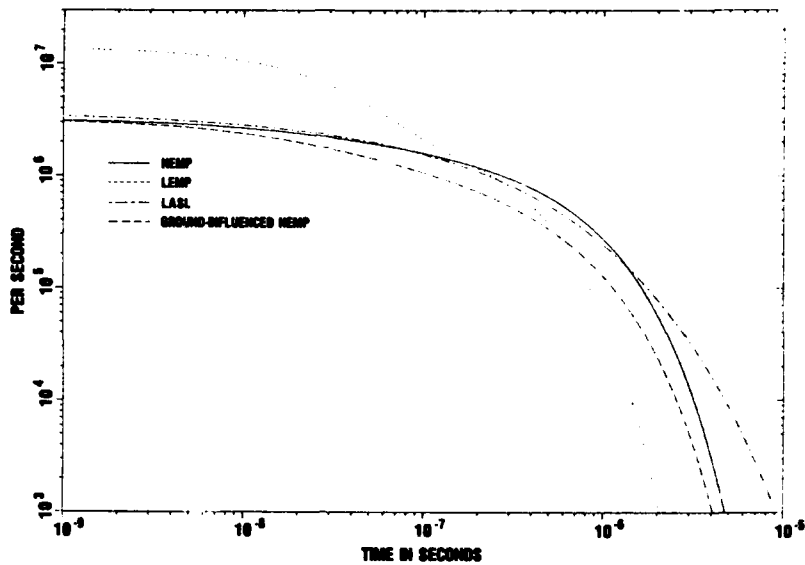


Figure 11. Time dependence of energy deposition buildup factors compared at 3000-m range for 1.5-MeV gamma rays.

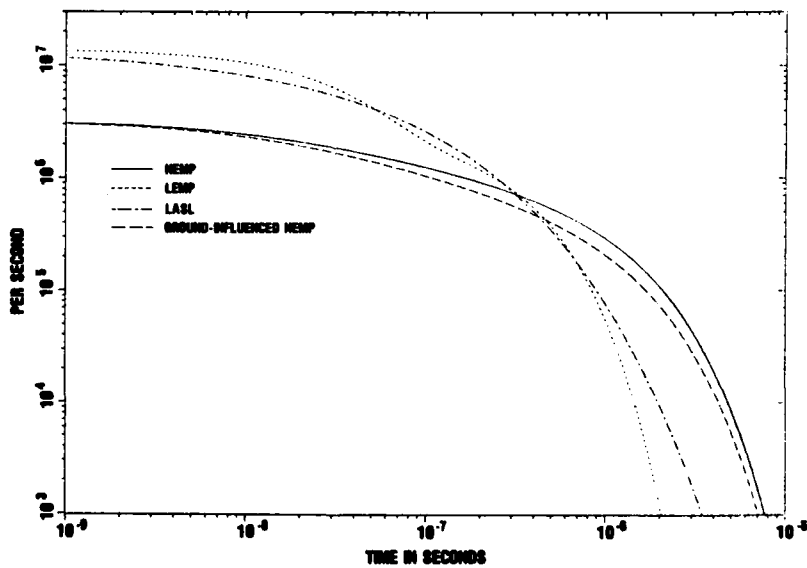


Figure 12. Time dependence of energy deposition buildup factors compared at 3000-m range for 5.0-MeV gamma rays.

Figures 7 to 9 show the energy deposition rate at a 300-m range for 0.5-, 1.5-, and 5.0-MeV source gamma ray energies. The agreement between the NEMP and LEMP drivers is good. Since the LEMP driver was based on close-in data, we expect it to be accurate at a 300-m range. The extremely close agreement at 1-ns retarded time is particularly encouraging and tends to confirm the correctness of the first-scatter part of the NEMP driver. The LASL curve seems to be concentrated too much toward early times, except for the 0.5-MeV curve.

Figures 10 to 12 show the energy deposition rate at a 3000-m range for 0.5-, 1.5-, and 5.0-MeV source gamma ray energies. At this deep penetration, we expect the LEMP curves to be concentrated too much toward early times in comparison with the NEMP curve--and they are. The NEMP and LASL curves agree well only for 1.5 MeV (fig. 11). For 5.0 MeV (fig. 12), the LASL curve is too close to the LEMP curve. Data shown in the LASL report<sup>7</sup> confirm a tendency of that curve fit to overestimate the energy deposition rate earlier than a fraction of a microsecond, for deep penetrations of about 10 attenuation lengths.

In all figures shown, the NEMP ground-influenced energy deposition rate begins equal to the NEMP free-field curve and later falls below by as much as a factor of about three for the 3000-m curve. For the 300-m curve, little difference is noted.

### 6.3 Time Dependence of Radial Compton Current

The ratio of radial Compton electron current to energy deposition rate is shown as a function of time for the NEMP, LEMP, and LASL drivers in figures 13 to 18. Figures 13 to 15 are for gamma ray energies of 0.5, 1.5, and 5.0 MeV at a range of 300 m from the burst. Figures 16 to 18 are for the same gamma ray energies at a range of 3000 m. The units of the ratios plotted are in Compton electron-meter per MeV. A factor of 0.8 has been separately applied to the LEMP and LASL drivers to account for multiple scattering of Compton electrons. This effect is already included in the NEMP driver. As for energy deposition rate, we expect the LEMP data to be more accurate at 300 m than at 3000 m. Good agreement is observed among all three curves (NEMP, LEMP, and LASL) at 300 m for each gamma ray energy, with a few exceptions. The NEMP curve is probably too high after about 1  $\mu$ s, although the significance of the discrepancy is slight in terms of the EMP that would be produced. Also, the LASL early time value for 0.5 MeV is high by more than a factor of two.

---

<sup>7</sup>J. S. Malik, E. D. Cashwell, and R. G. Schrandt, *The Time Dependence of the Compton Current and Energy Deposition from Scattered Gamma Rays*, Los Alamos Scientific Laboratory, NM, LA-7386-MS (July 1978).

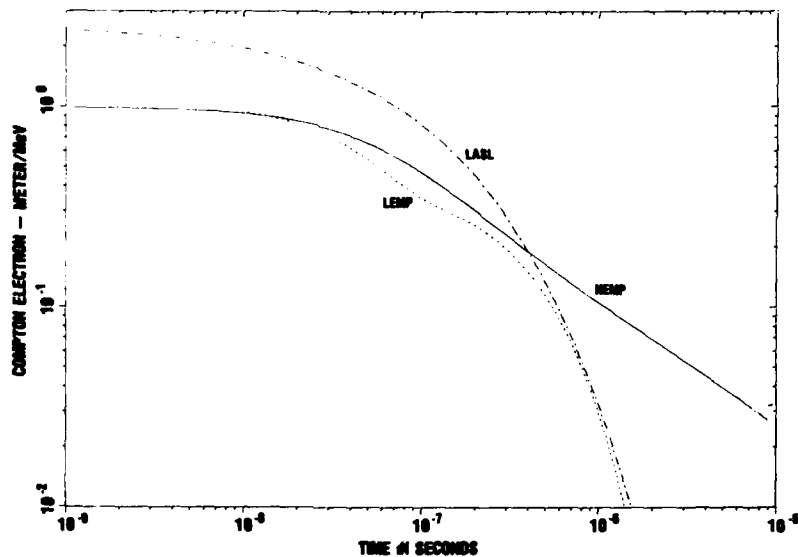


Figure 13. Time dependence compared for ratio of radial Compton electron current to energy deposition rate, at 300-m range for 0.5-MeV gamma rays.

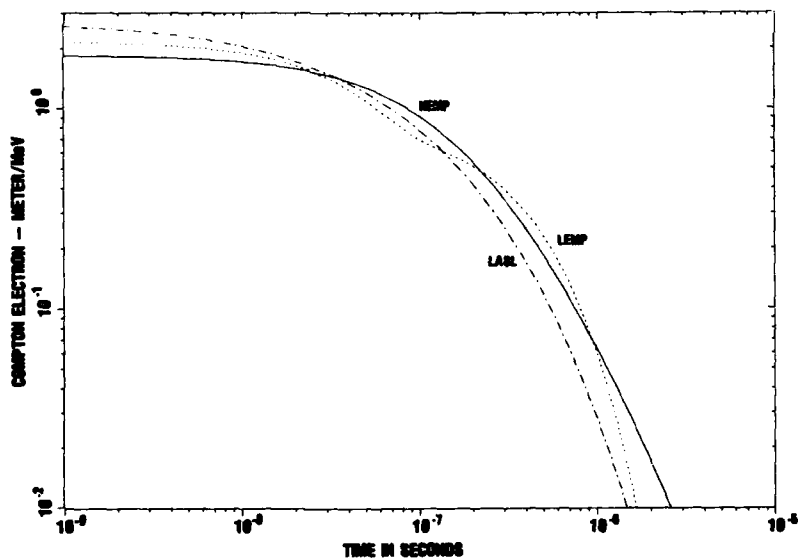


Figure 14. Time dependence compared for ratio of radial Compton electron current to energy deposition rate, at 300-m range for 1.5-MeV gamma rays.

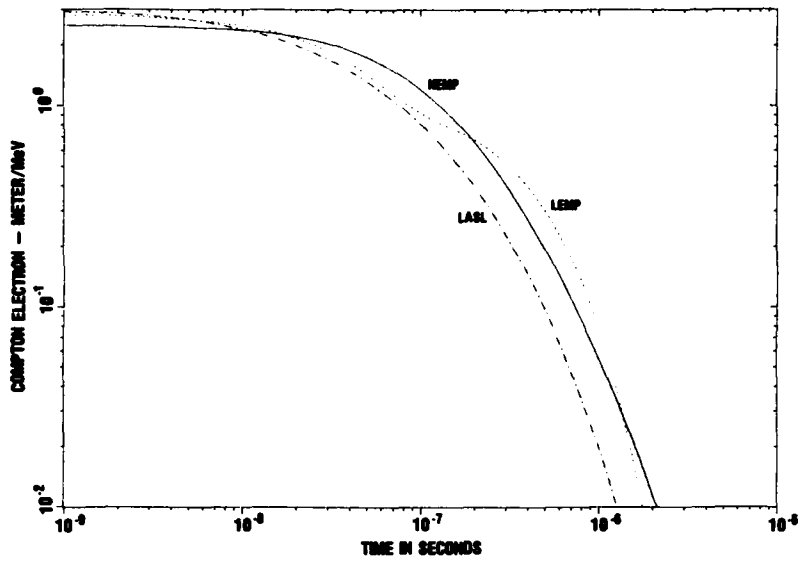


Figure 15. Time dependence compared for ratio of radial Compton electron current to energy deposition rate, at 300-m range for 5.0-MeV gamma rays.

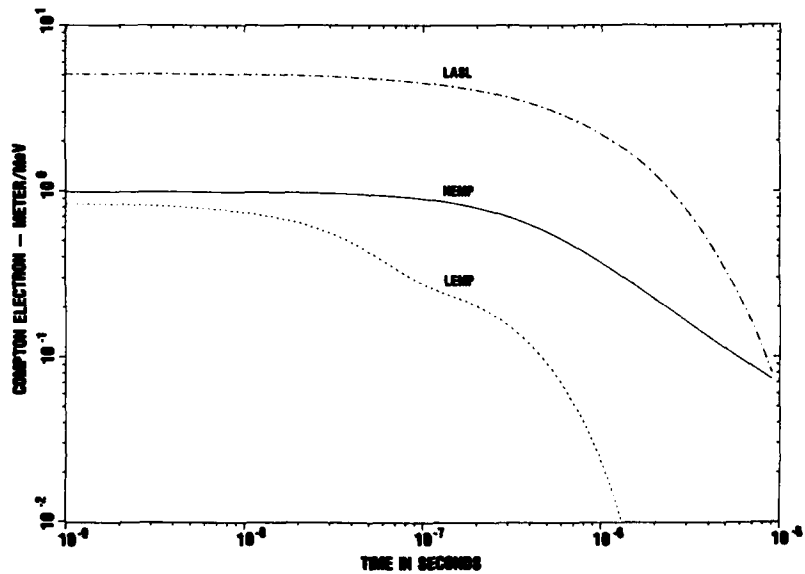


Figure 16. Time dependence compared for ratio of radial Compton electron current to energy deposition rate, at 3000-m range for 0.5-MeV gamma rays.

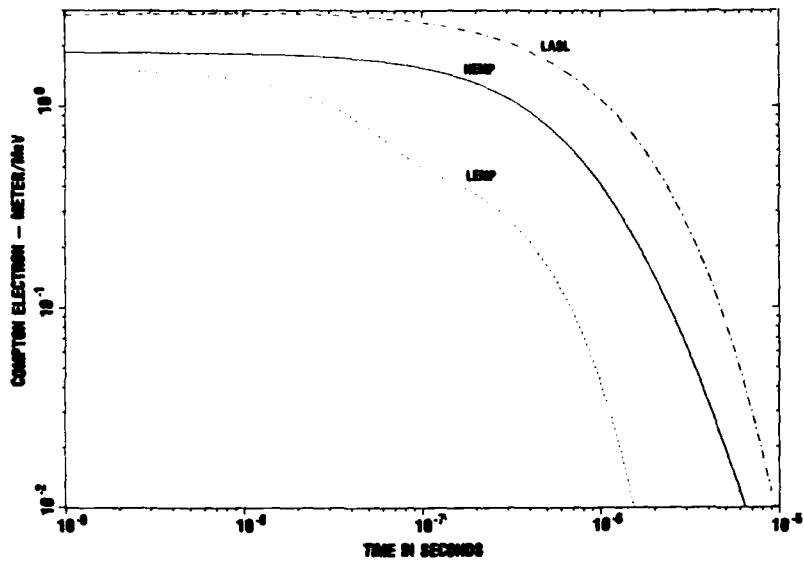


Figure 17. Time dependence compared for ratio of radial Compton electron current to energy deposition rate, at 3000-m range for 1.5-MeV gamma rays.

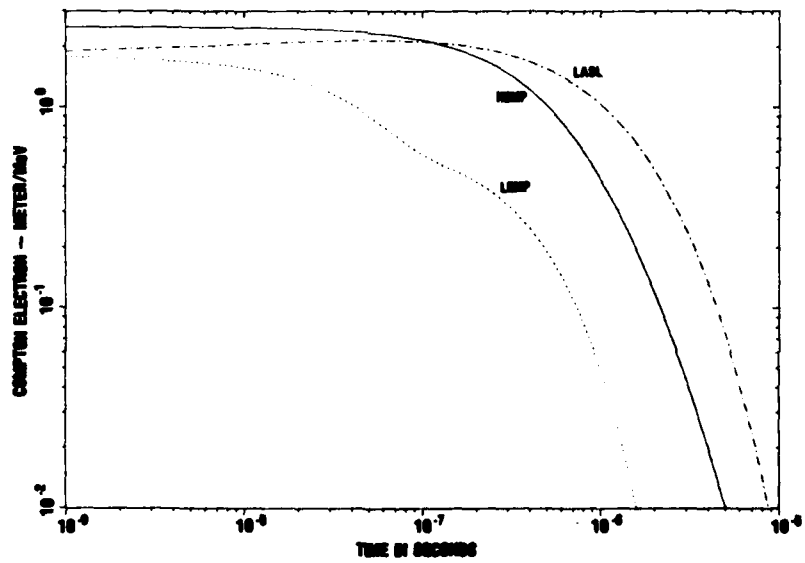


Figure 18. Time dependence compared for ratio of radial Compton electron current to energy deposition rate, at 3000-m range for 5.0-MeV gamma rays.

Agreement is worse at 3000 m for each gamma ray energy. The NEMP and LEMP curves are in fair agreement at early times, whereas the LASL curve is too high except for the 5.0-MeV curve. The LEMP curve decays much too fast, as expected at deep penetration where multiply scattered gamma rays retain more of their collimation than at shallow penetration. (The LEMP driver is based on shallow penetration data). The LASL curve, on the other hand, decays too slowly. Comparison of the NEMP curves with the Monte Carlo data that they were intended to fit reveals that the curves are usually somewhat too high after about 1  $\mu$ s, up to a factor of about two. However, considering the steepness of the curve, this error is not serious. No doubt a more complicated functional form would approximate the Monte Carlo data more faithfully.

From these comparisons, LEMP drivers would underestimate the Compton current at 3000 m by about a factor of four at 100 ns after the gamma-dot peak, for any of the gamma ray energies considered. The LASL drivers should not be applied to gamma ray energies less than 1.0 MeV, and they also significantly overestimate the Compton current at 3000 m for 1.5 MeV.

No ground effect on the ratio of Compton current to energy deposition rate was identified.

## 7. CONCLUDING REMARKS

This report presents improved calculations of EMP drivers due to a gamma ray point source in air over ground and analytic approximations to these EMP drivers. These were done for seven source gamma ray energies from 0.5 to 7.0 MeV. The EMP driver calculations were based on Monte Carlo simulation of the gamma ray transport using the SLEDGE computer code developed for this study. Notable features of the simulation included tracking to 25 attenuation lengths (mean free paths) penetration, presence of the earth, use of correlated sampling to estimate Compton electron currents more accurately, and extensive use of biasing and importance functions. The theoretical basis of the SLEDGE code is discussed. Significant aspects of the Monte Carlo results also are discussed.

The analytic approximations to the EMP drivers are described in detail, including (1) the energy deposition buildup factor (both free field and ground influenced), (2) time dependence of energy deposition as a function of both range from the burst and nearness to the ground, (3) ratio of radial Compton electron current to energy deposition rate, and (4) theta Compton electron current due to the presence of the ground. These approximations have been incorporated into an EMP driver software package used with the NEMP near-surface-burst EMP environment prediction code. Comparisons are made with two previous EMP driver

packages, one used in the LEMP surface-burst EMP environment prediction code and the other originated by LASL scientists for high-altitude burst problems. Free-field agreement with the LEMP drivers was generally good at short ranges. Free-field agreement with the LASL drivers was better at higher gamma ray energies. The new results predict ground effects as well, which were not considered by the LEMP and LASL researchers.

\*\*\*\*\*

#### LITERATURE CITED

- (1) H. J. Longley, C. L. Longmire, and K. S. Smith, Development of NEMP (U), Mission Research Corp., Santa Barbara, CA, HDL-CR-75-001-1 (April 1975). (SECRET--RESTRICTED DATA)
- (2) H. J. Longley and K. S. Smith, Developments in NEMP for 1977 (U), Mission Research Corp., Santa Barbara, CA, HDL-CR-77-0022-1 (January 1978). (SECRET--RESTRICTED DATA)
- (3) H. J. Longley and C. L. Longmire, Development and Testing of LEMP 1, Los Alamos Scientific Laboratory, NM, LA-4346 (April 1970).
- (4) L. L. Carter and E. D. Cashwell, Particle-Transport Simulation with the Monte Carlo Method, U.S. Energy Research and Development Administration TID-26607 (1975).
- (5) Milton Abramowitz and Irene Stegun, Handbook of Mathematical Functions, Dover Publications, Inc., New York (1965), 260.
- (6) William T. Wyatt, Jr., Transmission Factor Effects on the Average Forward Range of Compton Electrons, Harry Diamond Laboratories HDL-TM-80-10 (January 1980).
- (7) J. S. Malik, E. D. Cashwell, and R. G. Schrandt, The Time Dependence of the Compton Current and Energy Deposition from Scattered Gamma Rays, Los Alamos Scientific Laboratory, NM, LA-7386-MS (July 1978).

DISTRIBUTION

ADMINISTRATOR  
DEFENSE DOCUMENTATION CENTER  
ATTN DDC-TCA (12 COPIES)  
CAMERON STATION, BUILDING 5  
ALEXANDRIA, VA 22314

COMMANDER  
US ARMY RSCH & STD GP (EUR)  
ATTN LTC JAMES M. KENNEDY, JR.  
CHIEF, PHYSICS & MATH BRANCH  
PFO NEW YORK 09510

COMMANDER  
US ARMY ARMAMENT MATERIEL  
READINESS COMMAND  
ATTN DR SAR-LEP-L, TECHNICAL LIBRARY  
ROCK ISLAND, IL 61299

COMMANDER  
US ARMY MISSILE & MUNITIONS  
CENTER & SCHOOL  
ATTN ATSK-CTD-F  
REDSTONE ARSENAL, AL 35809

DIRECTOR  
US ARMY MATERIEL SYSTEMS  
ANALYSIS ACTIVITY  
ATTN DR XSY-MP  
ATTN DR XSY-PO  
ABERDEEN PROVING GROUND, MD 21005

DIRECTOR  
US ARMY BALLISTIC RESEARCH LABORATORY  
ATTN DR DAR-TSB-S (STINFO)  
ATTN DR XBR-AM, W. VANANTWERP  
ATTN DR STE-EL  
ATTN DR DAR-BLE  
ABERDEEN PROVING GROUND, MD 21005

U.S. ARMY ELECTRONICS TECHNOLOGY  
AND DEVICES LABORATORY  
ATTN DELET-DD  
FORT MONMOUTH, NJ 07703

TEXAS INSTRUMENTS, INC.  
P.O. BOX 226015  
ATTN FRANK POBLENZ,  
DALLAS, TX 75266

TELEDYNE BROWN ENGINEERING  
CUMMINGS RESEARCH PARK  
ATTN DR. MELVIN L. PRINCE, MS-44  
HUNTSVILLE, AL 35807

ENGINEERING SOCIETIES LIBRARY  
345 EAST 47TH STREET  
ATTN ACQUISITIONS DEPARTMENT  
NEW YORK, NY 10017

DIRECTOR  
ARMED FORCES RADIOBIOLOGY RESEARCH  
INSTITUTE  
DEFENSE NUCLEAR AGENCY  
NATIONAL NAVAL MEDICAL CENTER  
ATTN RESEARCH PROGRAM COORDINATING  
OFFICER  
BETHESDA, MD 20014

ASSISTANT TO THE SECRETARY OF DEFENSE  
ATOMIC ENERGY  
ATTN EXECUTIVE ASSISTANT  
WASHINGTON, DC 20301

DIRECTOR  
DEFENSE ADVANCED RSCH PROJ AGENCY  
ARCHITECT BUILDING  
ATTN TIO  
1400 WILSON BLVD.  
ARLINGTON, VA 22209

DIRECTOR  
DEFENSE CIVIL PREPAREDNESS AGENCY  
ASSISTANT DIRECTOR FOR RESEARCH  
ATTN ADMIN OFFICER  
ATTN RE (EO)  
ATTN PO (SE)  
WASHINGTON, DC 20301

DEFENSE COMMUNICATIONS ENGINEERING  
CENTER  
ATTN CODE R720, C. STANSBERRY  
ATTN CODE R123, TECH LIB  
ATTN CODE R400  
1860 WIEHLE AVENUE  
RESTON, VA 22090

DIRECTOR  
DEFENSE COMMUNICATIONS AGENCY  
ATTN CCTC C312  
ATTN CODE C313  
WASHINGTON, DC 20305

DIRECTOR  
DEFENSE INTELLIGENCE AGENCY  
ATTN RDS-3A  
ATTN RDS-3A4, POMPONIO PLAZA  
WASHINGTON, DC 20301

DIRECTOR  
DEFENSE NUCLEAR AGENCY  
ATTN RATN  
ATTN DDST  
ATTN RAEV  
ATTN TITL  
ATTN STVL  
ATTN VLIS  
WASHINGTON, DC 20305

COMMANDER  
FIELD COMMAND  
DEFENSE NUCLEAR AGENCY  
ATTN FCPR  
ATTN FCSPM, J. SMITH  
ATTN FCLMC  
KIRTLAND AFB, NM 87115

DIRECTOR  
INTERSERVICE NUCLEAR WEAPONS SCHOOL  
ATTN TTV  
KIRTLAND AFB, NM 87115

JOINT CHIEFS OF STAFF  
ATTN J-3  
WASHINGTON, DC 20301

DIRECTOR  
JOINT STRATEGIC TARGET PLANNING  
STAFF, JCS  
OFFUTT AFB  
ATTN JSAS  
ATTN JPST  
ATTN NRI-STINFO LIBRARY  
OMAHA, NE 68113

CHIEF  
LIVERMORE DIVISION  
FIELD COMMAND DNA  
DEPARTMENT OF DEFENSE  
LAWRENCE LIVERMORE LABORATORY  
P.O. BOX 808  
ATTN FCPRL  
LIVERMORE, CA 94550

NATIONAL COMMUNICATIONS SYSTEM  
OFFICE OF THE MANAGER  
DEPARTMENT OF DEFENSE  
ATTN NCS-TS, CHARLES D. BOGDON  
WASHINGTON, DC 20305

DIRECTOR  
NATIONAL SECURITY AGENCY  
DEPARTMENT OF DEFENSE  
ATTN R-52, O. VAN GUNTEN  
ATTN S232, D. VINCENT  
FT. MEADE, MD 20755

UNDER SECY OF DEF FOR RSCH & ENGRG  
DEPARTMENT OF DEFENSE  
ATTN G. BARSE  
ATTN S&SS (OS)  
WASHINGTON DC 20301

COMMANDER  
BMD SYSTEM COMMAND  
DEPARTMENT OF THE ARMY  
P.O. BOX 1500  
ATTN BMDSC-AOLIB  
HUNTSVILLE, AL 35807

COMMANDER  
ENADCOM TECHNICAL SUPPORT ACTIVITY  
DEPARTMENT OF THE ARMY  
ATTN DELCS-K, A COHEN  
ATTN DELET-IR, E. HUNTER  
FORT MONMOUTH, NJ 07703

COMMANDER  
US ARMY ARMOR CENTER  
ATTN TECHNICAL LIBRARY  
FORT KNOX, KY 40121

COMMANDER  
US ARMY COMM-ELEC ENGRG INSTAL  
AGENCY  
ATTN CCC-PRSO-S  
ATTN CCC-CED-SES  
FT HUACHUCA, AZ 85613

COMMANDER  
US ARMY COMMUNICATIONS COMMAND  
COMBAT DEVELOPMENT DIVISION  
ATTN ATSI-CD-MD  
FT. HUACHUCA, AZ 85613

DISTRIBUTION (Cont'd)

CHIEF  
US ARMY COMMUNICATIONS SYS AGENCY  
ATTN CCM-RD-T CCM-AD-SV  
FORT MONMOUTH, NJ 07703

PROJECT OFFICER  
US ARMY COMMUNICATIONS RES &  
DEV COMMAND  
ATTN DRCPM-ATC  
ATTN DRCPM-TDS-BSI  
FORT MONMOUTH, NJ 07703

DIVISION ENGINEER  
US ARMY ENGINEER DIV HUNTSVILLE  
P.O. BOX 1600, WEST STATION  
ATTN HNDED-SR  
ATTN A. T. BOLT  
HUNTSVILLE, AL 35807

US ARMY INTEL THREAT ANALYSIS  
DETACHMENT  
ROOM 2201, BLDG A  
ARLINGTON HALL STATION  
ATTN RM 2200, BLDG A  
ARLINGTON, VA 22212

COMMANDER  
US ARMY INTELLIGENCE & SEC CMD  
ARLINGTON HALL STATION  
4000 ARLINGTON BLVD  
ATTN TECHNICAL LIBRARY  
ATTN TECH INFO PAC  
ARLINGTON, VA 22212

COMMANDER  
US ARMY MISSILE RESEARCH  
& DEVELOPMENT COMMAND  
ATTN DRCPM-PE-EA, WALLACE O. WAGNER  
ATTN DRCPM-PE-EG, WILLIAM B. JOHNSON  
ATTN DRDMI-TBD  
ATTN DRDMI-EAA  
REDSTONE ARSENAL, AL 35809

US ARMY NUCLEAR & CHEMICAL AGENCY  
7500 BACKLICK ROAD  
BUILDING 2073  
ATTN COL A. LOWRY  
ATTN DR. J. BERBERET  
SPRINGFIELD, VA 22150

COMMANDER  
US ARMY TEST AND EVALUATION COMMAND  
ATTN DRSTE-FA  
ABERDEEN PROVING GROUND, MD 21005

COMMANDER  
US ARMY TRAINING AND  
DOCTRINE COMMAND  
ATTN ATORI-OP-SW  
FORT MONROE, VA 23651

COMMANDER  
WHITE SANDS MISSILE RANGE  
DEPARTMENT OF THE ARMY  
ATTN STEWS-TE-AN, J. OKUMA  
WHITE SANDS MISSILE RANGE, NM 88002

OFFICER-IN-CHARGE  
CIVIL ENGINEERING LABORATORY  
NAVAL CONSTRUCTION BATTALION CENTER  
ATTN CODE LOBA (LIBRARY)  
ATTN CODE LOBA  
PORT HUENEME, CA 93041

COMMANDER  
NAVAL AIR SYSTEMS COMMAND  
ATTN AIR-350F  
WASHINGTON, DC 21360

COMMANDER  
NAVAL ELECTRONIC SYSTEMS COMMAND  
ATTN PME 117-215  
WASHINGTON, DC 20360

COMMANDER  
NAVAL OCEAN SYSTEMS CENTER  
ATTN CODE 015, C. FLETCHER  
ATTN RESEARCH LIBRARY  
ATTN CODE 7240, S. W. LICHTMAN  
SAN DIEGO, CA 92152

COMMANDING OFFICER  
NAVAL ORDNANCE STATION  
ATTN STANDARDIZATION DIV  
INDIAN HEAD, MD 20640

SUPERINTENDENT (CODE 1424)  
NAVAL POSTGRADUATE SCHOOL  
ATTN CODE 1424  
MONTEREY, CA 93940

DIRECTOR  
NAVAL RESEARCH LABORATORY  
ATTN CODE 4104, EMANUAL L. BRANCATO  
ATTN CODE 2627, DORIS R. FOLEN  
ATTN CODE 6623, RICHARD L. STATLER  
ATTN CODE 6624  
WASHINGTON, DC 20375

COMMANDER  
NAVAL SHIP ENGINEERING CENTER  
DEPARTMENT OF THE NAVY  
ATTN CODE 6174D2, EDWARD F. DUFFY  
WASHINGTON, DC 20362

COMMANDER  
NAVAL SURFACE WEAPONS CENTER  
ATTN CODE F32, EDWIN R. RATHBURN  
ATTN L. LIBELLO, CODE WR43  
ATTN CODE WA51RH, RM 130-108  
WHITE OAK, SILVER SPRING, MD 20910

COMMANDER  
NAVAL SURFACE WEAPONS CENTER  
DAHLGREN LABORATORY  
ATTN CODE DF-56  
DAHLGREN, VA 22448

COMMANDER  
NAVAL WEAPONS CENTER  
ATTN CODE 533, TECH LIB  
CHINA LAKE, CA 93555

COMMANDING OFFICER  
NAVAL WEAPONS EVALUATION FACILITY  
KIRTLAND AIR FORCE BASE  
ATTN CODE AT-6  
ALBUQUERQUE, NM 87117

OFFICE OF NAVAL RESEARCH  
ATTN CODE 427  
ARLINGTON, VA 22217

DIRECTOR  
STRATEGIC SYSTEMS PROJECT OFFICE  
NAVY DEPARTMENT  
ATTN NSP-2701, JOHN W. FITSBERGER  
ATTN NSP-2342, RICHARD L. COLEMAN  
ATTN NSP-43, TECH LIB  
ATTN NSP-27334  
ATTN NSP-230, D. GOLD  
WASHINGTON, DC 20376

COMMANDER  
AERONAUTICAL SYSTEMS DIVISION, AFSC  
ATTN ASD-YH-EX  
ATTN ENFTV  
WRIGHT-PATTERSON AFB, OH 45333

AIR FORCE TECHNICAL APPLICATIONS  
CENTER  
ATTN TFS, M. SCHNEIDER  
PATRICK AFB, FL 32925

AF WEAPONS LABORATORY, AFSC  
ATTN NTN  
ATTN NT  
ATTN EL, CARL E. BAUM,  
ATTN ELXT  
ATTN SUL  
ATTN CA  
ATTN ELA, J. P. CASTILLO  
ATTN ELP  
ATTN ELT, W. PAGE  
ATTN NXS  
KIRTLAND AFB, NM 87117

DIRECTOR  
AIR UNIVERSITY LIBRARY  
DEPARTMENT OF THE AIR FORCE  
ATTN AUL-LSE-70-250  
MAXWELL AFB, AL 36112

HEADQUARTERS  
ELECTRONIC SYSTEMS DEVISION/YSEA  
DEPARTMENT OF THE AIR FORCE  
ATTN YSEA  
HANSCOM AFB, MA 01731

COMMANDER  
FOREIGN TECHNOLOGY DIVISION, AFSC  
ATTN NICD LIBRARY  
ATTN EYDP, B. L. BALLARD  
WRIGHT-PATTERSON AFB, OH 45433

COMMANDER  
ODGEN ALC/MMEDDE  
DEPARTMENT OF THE AIR FORCE  
ATTN OO-ALC/METH, P. W. BERTHEL  
ATTN MMEDO, LEO KIMMAN  
ATTN MAJ R. BLACKBURN  
HILL AFB, UT 84406

DISTRIBUTION (Cont'd)

COMMANDER  
ROME AIR DEVELOPMENT CENTER AFSC  
ATTN TSLD  
GRIFFISS AFB, NY 13441

COMMANDER  
SACRAMENTO AIR LOGISTICS CENTER  
DEPARTMENT OF THE AIR FORCE  
ATTN MMCRS, H. A. PELMASTRO  
ATTN MMIRA, J. W. DEMES  
ATTN MMSRM, F. R. SPEAR  
MCLELLAN AFB, CA 95652

SAMSO/IN  
AIR FORCE SYSTEMS COMMAND  
POST OFFICE BOX 92960  
WORLDWAY POSTAL CENTER  
(INTELLIGENCE)  
ATTN IND  
LOS ANGELES, CA 90009

SAMSO/MN  
AIR FORCE SYSTEMS COMMAND  
(MINUTEMAN)  
ATTN MNMH, MAJ M. BARAN  
ATTN MNMH, CAPT R. I. LAWRENCE  
NORTON AFB, CA 92409

SAMSO/YA  
AIR FORCE SYSTEMS COMMAND  
POST OFFICE BOX 92960  
WORLDWAY POSTAL CENTER  
ATTN YAPC  
LOS ANGELES, CA 90009

STRATEGIC AIR COMMAND/XPFS  
ATTN NRI-STINFO LIBRARY  
ATTN DEL  
ATTN GARNET E. MATZKE  
ATTN XPFS, MAJ BRIAN G. STEPHEN  
OPPUTT AFB, NE 68113

DEPARTMENT OF ENERGY  
ALBUQUERQUE OPERATIONS OFFICE  
P.O. BOX 5400  
ATTN DOC CON FOR TECH LIBRARY  
ATTN OPERATIONAL SAFETY DIV  
ALBUQUERQUE, NM 87115

UNIVERSITY OF CALIFORNIA  
LAWRENCE LIVERMORE LABORATORY  
P.O. BOX 808  
ATTN DOC CON FOR TECHNICAL  
INFORMATION DEPT  
ATTN DOC CON FOR L-06, T. DONICH  
ATTN DOC CON FOR L-545, D. MEEKER  
ATTN DOC CON FOR L-156, E. MILLER  
ATTN DOC CON FOR L-10, H. KRUGER  
ATTN DOC CON FOR H. S. CABAYAN  
LIVERMORE, CA 94550

LOS ALAMOS SCIENTIFIC LABORATORY  
P.O. BOX 1663  
ATTN DOC CON FOR BRUCE W. NOEL  
ATTN DOC CON FOR CLARENCE BENTON  
LOS ALAMOS, NM 87545

SANDIA LABORATORIES  
P.O. BOX 5800  
ATTN DON CON FOR C. N. VITTITOE  
ATTN DON CON FOR R. L. PARKER  
ATTN DOC CON FOR ELMER F. HARTMAN  
ALBUQUERQUE, NM 87115

CENTRAL INTELLIGENCE AGENCY  
ATTN RD/SI, RM 5G48, HQ BLDG  
FOR OSI/NED/NWB  
WASHINGTON, DC 20505

ADMINISTRATOR  
DEFENSE ELECTRIC POWER ADMIN  
DEPARTMENT OF THE INTERIOR  
INTERIOR SOUTH BLDG, 312  
ATTN L. O'NEILL  
WASHINGTON, DC 20240

DEPARTMENT OF TRANSPORTATION  
FEDERAL AVIATION ADMINISTRATION  
HEADQUARTERS SEC DIV, ASE-300  
800 INDEPENDENCE AVENUE, SW  
ATTN SEC DIV ASE-300  
WASHINGTON, DC 20591

AEROSPACE CORPORATION  
P.O. BOX 92957  
ATTN C. B. PEARLSTON  
ATTN IRVING M. GARFUNKEL  
ATTN JULIAN REINHEIMER  
ATTN LIBRARY  
ATTN CHARLES GREENHOW  
LOS ANGELES, CA 90009

AGBABIAN ASSOCIATES  
250 NORTH NASH STREET  
ATTN LIBRARY  
EL SEGUNDO, CA 90245

AVCO RESEARCH & SYSTEMS GROUP  
201 LOWELL STREET  
ATTN W. LEPSEVICH  
WILMINGTON, MA 01887

BATTELLE MEMORIAL INSTITUTE  
505 KING AVENUE  
ATTN ROBERT H. BALZEK  
ATTN EUGENE R. LEACH  
COLUMBUS, OH 43201

BDM CORPORATION  
7915 JONES BRANCH DRIVE  
ATTN CORPORATE LIBRARY  
MCLEAN, VA 22101

BDM CORPORATION  
P.O. BOX 9274  
ALBUQUERQUE INTERNATIONAL  
ATTN LIB  
ALBUQUERQUE, NM 87119

BENDIX CORPORATION, THE  
RESEARCH LABORATORIES DIVISION  
BENDIX CENTER  
ATTN MAX FRANK  
SOUTHFIELD, MI 48075

BENDIX CORPORATION  
NAVIGATION AND CONTROL GROUP  
ATTN DEPT 6401  
TETERBORO, NJ 07608

BOEING COMPANY  
P.O. BOX 3707  
ATTN HOWARD W. WICKLEIN  
ATTN D. E. ISBELL  
ATTN DAVID KEMLE  
ATTN B. C. HANRAHAN  
ATTN KENT TECH LIB  
SEATTLE, WA 98124

BOOZ-ALLEN AND HAMILTON, INC.  
106 APPLE STREET  
ATTN R. J. CHRISNER  
ATTN TECH LIB  
TINTON FALLS, NJ 07724

BURROUGHS CORPORATION  
FEDERAL AND SPECIAL SYSTEMS GROUP  
CENTRAL AVE AND ROUTE 252  
P.O. BOX 517  
ATTN ANGELO J. MAURIELLO  
PAOLI, PA 19301

CALSPAN CORPORATION  
P.O. BOX 400  
ATTN TECH LIBRARY  
BUFFALO, NY 14225

CHARLES STARK DRAPER LABORATORY INC.  
555 TECHNOLOGY SQUARE  
ATTN KENNETH FERTIG  
ATTN TIC MS 74  
CHAMBRIDGE, MA 02139

CINCINNATI ELECTRONICS CORPORATION  
2630 GLENDALE-HILFORD ROAD  
ATTN LOIS HAMMOND  
CINCINNATI, OH 45241

COMPUTER SCIENCES CORPORATION  
6565 ARLINGTON BLVD  
ATTN RAMONA BRIGGS  
FALLS CHURCH, VA 22046

COMPUTER SCIENCES CORPORATION  
1400 SAN MATEO BLVD, SE  
ATTN RICHARD H. DICKHAUT  
ATTN ALVIN SCHIFF  
ALBUQUERQUE, NM 87108

CONTROL DATA CORPORATION  
P.O. BOX 0  
ATTN JACK MEEHAN  
MINNEAPOLIS, MN 55440

CUTLER-HAMMER, INC.  
AIL DIVISION  
COMAC ROAD  
ATTN EDWARD KARPEN  
DEER PARK, NY 11729

DIKEMOOD INDUSTRIES, INC  
1009 BRANDSBURY DRIVE, SE  
ATTN TECH LIB  
ATTN L. WAYNE DAVIS  
ALBUQUERQUE, NM 87106

DISTRIBUTION (Cont'd)

DIKWOOD INDUSTRIES, INC.  
1100 GLENDON AVENUE  
ATTN K. LEE  
LOS ANGELES, CA 90024

E-SYSTEMS, INC  
GREENVILLE DIVISION  
P.O. BOX 1056  
ATTN JOLETA MOORE  
GREENVILLE, TX 75401

EFFECTS TECHNOLOGY, INC.  
5383 HOLLISTER AVENUE  
ATTN S. CLOW  
SANTA BARBARA, CA 93111

EG&G WASHINGTON ANALYTICAL  
SERVICES CENTER, INC.  
P.O. BOX 10218  
ATTN C. GILES  
ALBUQUERQUE, NM 87114

ECON NUCLEAR COMPANY, INC.  
RESEARCH AND TECHNOLOGY CENTER  
2955 GEORGE WASHINGTON WAY  
ATTN DR. A. W. TRIVELPIECE  
RICHLAND, WA 99352

FAIRCHILD CAMERA AND INSTRUMENT CORP  
464 ELLIS STREET  
ATTN SEC CON FOR DAVID K. MYERS  
MOUNTAIN VIEW, CA 94040

FORD AEROSPACE & COMMUNICATIONS CORP  
3939 FABIAN WAY  
ATTN TECHNICAL LIBRARY  
PALO ALTO, CA 94303

FORD AEROSPACE & COMMUNICATIONS OPERATIONS  
FORD & JAMBOREE ROADS  
ATTN KEN C. ATTINGER  
ATTN E. R. PONCELET, JR.  
NEWPORT BEACH, CA 92663

FRANKLIN INSTITUTE, THE  
20TH STREET AND PARKWAY  
ATTN RAMIE H. THOMPSON  
PHILADELPHIA, PA 19103

GENERAL DYNAMICS CORP  
ELECTRONICS DIVISION  
P.O. BOX 81125  
ATTN RSCH LIB  
SAN DIEGO, CA 92138

GENERAL DYNAMICS CORPORATION  
INTER-DIVISION RESEARCH LIBRARY  
KEARNY MESA  
P.O. BOX 80847  
ATTN RESEARCH LIBRARY  
SAN DIEGO, CA 98123

GENERAL ELECTRIC CO.-TEMPO  
CENTER FOR ADVANCED STUDIES  
816 STATE STREET (PO DRAWER QQ)  
ATTN DASIAC  
ATTN ROYDEN R. RUTHERFORD  
ATTN WILLIAM MCNAMERA  
SANTA BARBARA, CA 93102

GENERAL ELECTRIC COMPANY  
AEROSPACE ELECTRONICS SYSTEMS  
FRENCH ROAD  
ATTN CHARLES M. HEWISON  
UTICA, NY 13503

GENERAL ELECTRIC COMPANY  
P.O. BOX 5000  
ATTN TECH LIB  
BINGHAMTON, NY 13902

GENERAL ELECTRIC CO.-TEMPO  
ALEXANDRIA OFFICE  
HUNTINGTON BUILDING, SUITE 300  
2560 HUNTINGTON AVENUE  
ATTN DASIAC  
ALEXANDRIA, VA 22303

GENERAL RESEARCH CORPORATION  
SANTA BARBARA  
P.O. BOX 6770  
ATTN TECH INFO OFFICE  
SANTA BARBARA, CA 93111

GEORGIA INSTITUTE OF TECHNOLOGY  
GEORGIA TECH RESEARCH INSTITUTE  
ATTN R. CURRY  
ATLANTA, GA 30332

GEORGIA INSTITUTE OF TECHNOLOGY  
OFFICE OF CONTRACT ADMINISTRATION  
ATTN RES & SEC COORD FOR HUGH DENNY  
ATLANTA, GA 30332

GRUMMAN AEROSPACE CORPORATION  
SOUTH OYSTER BAY ROAD  
ATTN L-01 35  
BETHPAGE, NY 11714

GTE SYLVANIA INC.  
ELECTRONICS SYSTEMS GRP-EASTERN DIV  
77 A STREET  
ATTN CHARLES A. THORNHILL, LIBRARIAN  
ATTN LEONARD L. BLAISDELL  
NEEDHAM, MA 02194

GTE SYLVANIA, INC.  
189 B STREET  
ATTN CHARLES H. RAMSBOTTOM  
ATTN DAVID D. FLOOD  
ATTN EMIL P. MOTCHOK  
ATTN H & V GROUP, MARIO A. NUREFORA  
ATTN J. WALDRON  
NEEDHAM HEIGHTS, MA 02194

HARRIS CORPORATION  
HARRIS SEMICONDUCTOR DIVISION  
P.O. BOX 883  
ATTN V PRES & MGR PRGMS DIV  
MELBOURNE, FL 32901

HAZELTINE CORPORATION  
PULASKI ROAD  
ATTN TECH INFO CTR, M. WAITE  
GREENLAW, NY 11740

HONEYWELL INCORPORATED  
AVIONICS DIVISION  
2600 RIDGEWAY PARKWAY  
ATTN S&RC LIB  
ATTN RONALD R. JOHNSON  
MINNEAPOLIS, MN 55413

HONEYWELL INCORPORATED  
AVIONICS DIVISION  
13350 U.S. HIGHWAY 19 NORTH  
ATTN M.S. 725-5, STACEY H. GRAFF  
ATTN W. E. STEWART  
ST. PETERSBURG, FL 33733

HUGHES AIRCRAFT COMPANY  
CENTINELA AND TEALE  
ATTN JOHN B. SINGLETARY  
ATTN CTDC 6/E110  
ATTN KENNETH R. WALKER  
CULVER CITY, CA 90230

IIT RESEARCH INSTITUTE  
ELECTROMAG COMPATABILITY ANAL CTR  
NORTH SEVERN  
ATTN ACOAT  
ANNAPOLIS, MD 21402

IIT RESEARCH INSTITUTE  
10 WEST 35TH STREET  
ATTN IRVING N. MINDEL  
ATTN JACK E. BRIDGES  
CHICAGO, IL 60616

INSTITUTE FOR DEFENSE ANALYSES  
400 ARMY-NAVY DRIVE  
ATTN TECH INFO SERVICES  
ARLINGTON, VA 22202

INTL TEL & TELEGRAPH CORPORATION  
500 WASHINGTON AVENUE  
ATTN TECHNICAL LIBRARY  
ATTN ALEXANDER T. RICHARDSON  
NUTLEY, NJ 07110

IRT CORPORATION  
P.O. BOX 81087  
ATTN C. B. WILLIAMS  
ATTN DENNIS SWIFT  
SAN DIEGO, CA 92138

JAYCOR  
SANTA BARBARA FACILITY  
P.O. BOX 2008  
ATTN W. A. RADASKY  
SANTA BARBARA, CA 93120

JAYCOR  
1401 CAMINO DEL MAR  
ATTN ERIC P. WENAAS  
ATTN RALPH H. STAHL  
DEL MAR, CA 92014

JAYCOR  
205 S WHITING STREET, SUITE 500  
ATTN LIB  
ALEXANDRIA, VA 22304

DISTRIBUTION (Cont'd)

KAMAN SCIENCES CORPORATION  
1500 GARDEN OF THE GODS ROAD  
ATTN ALBERT P. BRIDGES  
ATTN W. FOSTER RICH  
ATTN WALTER E. WARE  
ATTN FRANK H. SHELTON  
ATTN JERRY I. LUBELL  
ATTN PHIL TRACY  
ATTN WERNER STARK  
COLORADO SPRINGS, CO 80907

LITTON SYSTEMS, INC.  
DATA SYSTEMS DIVISION  
8000 WOODLEY AVENUE  
ATTN EMC GP  
ATTN M848-61  
VAN NUYS, CA 91409

LITTON SYSTEMS, INC.  
AMECOM DIVISION  
5115 CALVERT ROAD  
ATTN J. SKAGGS  
COLLEGE PARK, MD 20740

LOCKHEED MISSILES AND SPACE COMPANY, INC  
P.O. BOX 504  
ATTN L. ROSSI  
ATTN SAMUEL I. TAIMUTY  
ATTN H. E. THAYN  
ATTN GEORGE F. HEATH  
ATTN BENJAMIN T. KIMURA  
SUNNYVALE, CA 94086

LOCKHEED MISSILES AND SPACE COMPANY, INC.  
3251 HANOVER STREET  
ATTN TECH INFO CTR D/COLL  
PALO ALTO, CA 94304

M.I.T. LINCOLN LABORATORY  
P.O. BOX 73  
ATTN LEONA LOUGHLIN  
LEXINGTON, MA 02173

MARTIN MARIETTA CORPORATION  
ORLANDO DIVISION  
P.O. BOX 5837  
ATTN MONA C. GRIFFITH  
ORLANDO, FL 32805

MCDONNELL DOUGLAS CORPORATION  
POST OFFICE BOX 516  
ATTN TOM ENDER  
ST. LOUIS, MO 63166

MCDONNELL DOUGLAS CORPORATION  
5301 BOLSA AVENUE  
ATTN STANLEY SCHNEIDER  
ATTN TECH LINRARY SERVICES  
HUNTINGTON BEACH, CA 92647

MISSION RESEARCH CORPORATION  
P.O. DRAWER 719  
ATTN BMP GROUP  
ATTN WILLIAM C. HART  
ATTN C. LONGMIRE  
SANTA BARBARA, CA 93102

MISSION RESEARCH CORPORATION  
EM SYSTEM APPLICATIONS DIVISION  
1400 SAN MATEO BLVD, SE, SUITE A  
ATTN DAVID E. HEREWETHER  
ATTN L. N. MCCORMICK  
ALBUQUERQUE, NM 87108

MISSION RESEARCH CORPORATION-SAN DIEGO  
P.O. BOX 1209  
ATTN V. A. J. VAN LINT  
LA JOLLA, CA 92038

MITRE CORPORATION, THE  
P.O. BOX 208  
ATTN M. F. FITZGERALD  
BEDFORD, MA 01730

NORDEN SYSTEMS, INC.  
HELEN STREET  
ATTN TECHNICAL LIBRARY  
NORWALK, CT 06856

NORTHROP RESEARCH TECHNOLOGY CENTER  
ONE RESEARCH PARK  
ATTN LIBRARY  
PALOS VERDES PENN, CA 90274

NORTHROP CORPORTION  
ELECTRONIC DIVISION  
2301 WEST 120TH STREET  
ATTN LEW SMITH  
ATTN RAD EFFECTS GRP  
HAWTHORNE, CA 90250

PHYSICS INTERNATIONAL COMPANY  
2700 MERCED STREET  
ATTN DOC CON  
SAN LEANDRO, CA 94577

R.&D ASSOCIATED  
P.O. BOX 9695  
ATTN S. CLAY ROGERS  
ATTN RICHARD R. SCHAEFER  
ATTN DOC CON  
ATTN M. GROVER  
ATTN C. MACDONALD  
MARINA DEL REY, CA 90291

R&D ASSOCIATES  
1401 WILSON BLVD  
SUITE 500  
ATTN J. COMBARDT  
ARLINGTON, VA 22209

RAND CORPORATION  
1700 MAIN STREET  
ATTN LIB-D  
ATTN W. SOLLFREY  
SANTA MONICA, CA 90406

RAYTHEON COMPANY  
HARTWELL ROAD  
ATTN GAJANAN R. JOSI  
BEDFORD, MA 01730

RAYTHEON COMPANY  
528 BOSTON POST ROAD  
ATTN HAROLD L. FLESCHER  
SUDBURY, MA 01776

RCA CORPORATION  
GOVERNMENT SYSTEMS DIVISION  
ASTRO ELECTRONICS  
P.O. BOX 800, LOCOST CORNER  
EAST WINDSOR TOWNSHIP  
PRINCETON, NJ 08540

RCA CORPORATION  
DAVID SARNOFF RESEARCH CENTER  
P.O. BOX 432  
ATTN SECURITY DEPT, L. MINICH  
PRINCETON, NJ 08540

RCA CORPORATION  
CAMDEN COMPLEX  
FRONT & COOPER STREETS  
ATTN OLIVE WHITEHEAD  
ATTN R. W. TOSTROM  
CAMDEN, NJ 08012

ROCKWELL INTERNATIONAL CORPORATION  
P.O. BOX 3105  
ATTN N. J. RUDIE  
ATTN J. L. MONROE  
ATTN V. J. MICHEL  
ATTN D/243-068, 031-CA31  
ANAHEIM, CA 92803

ROCKWELL INTERNATIONAL CORPORATION  
SPACE DIVISION  
12214 SOUTH LAKEWOOD BOULEVARD  
ATTN B. E. WHITE  
DOWNEY, CA 90241

ROCKWELL INTERNATIONAL CORPORATION  
815 LAPAUM STREET  
ATTN B-1, DIV TIC (BAOB)  
EL SEGUNDO, CA 90245

ROCKWELL INTERNATIONAL CORPORATION  
P.O. BOX 369  
ATTN F. A. SHAW  
CLEARFIELD, UT 84015

SANDERS ASSOCIATES, INC.  
95 CANAL STREET  
ATTN 1-6270, R. G. DESPATHY, SR P E  
NASHUA, NH 03060

SCIENCE APPLICATIONS, INC.  
P.O. BOX 277  
ATTN FREDERICK M. TESCHE  
BERKELEY, CA 94701

SCIENCE APPLICATIONS, INC.  
P.O. BOX 2351  
ATTN R. PARKINSON  
LA JOLLA, CA 92038

SCIENCE APPLICATIONS, INC.  
HUNTSVILLE DIVISION  
2109 W. CLINTON AVENUE  
SUITE 700  
ATTN NOEL R. BYRN  
HUNTSVILLE, AL 35805

SCIENCE APPLICATIONS, INC.  
8400 WESTPARK DRIVE  
ATTN WILLIAM L. CHADSEY  
MCLEAN, VA 22101

DISTRIBUTION (Cont'd)

SINGER COMPANY  
ATTN: SECURITY MANAGER  
FOR TECH INFO CTR  
1150 MC BRIDE AVENUE  
LITTLE FALLS, NJ 07424

SPERRY RAND CORPORATION  
SPERRY MICROWAVE ELECTRONICS  
P.O. BOX 4648  
ATTN MARGARET CORT  
CLEARWATER, FL 33518

SPERRY RAND CORPORATION  
SPERRY DIVISION  
MARCUS AVENUE  
ATTN TECH LIB  
GREAT NECK, NY 11020

SPERRY RAND CORPORATION  
SPERRY FLIGHT SYSTEMS  
P.O. BOX 21111  
ATTN D. ANDREW SCHOW  
PHOENIX, AZ 85036

SPIRE CORPORATION  
P.O. BOX D  
ATTN JOHN R. UGLUM  
ATTN ROGER G. LITTLE  
BEDFORD, MA 01730

SRI INTERNATIONAL  
333 RAVENSWOOD AVENUE  
ATTN ARTHUR LEE WHITSON  
MENLO PARK, CA 94025

SYSTEMS, SCIENCE AND SOFTWARE, INC.  
P.O. BOX 1620  
ATTN ANDREW R. WILSON  
LA JOLLA, CA 92038

TEXAS INSTRUMENTS, INC.  
P.O. BOX 6015  
ATTN TECH LIB  
ATTN DONALD J. MANUS  
DALLAS, TX 75265

TW DEFENSE & SPACE SYS GROUP  
ONE SPACE PARK  
ATTN O. E. ADAMS  
ATTN R. K. FLEBUCH  
ATTN L. R. MAGNOLIA  
ATTN H. H. HOLLOWAY  
ATTN W. GARGARO  
REDONDO BEACH, CA 90278

TEXAS TECH UNIVERSITY  
P.O. BOX 5404 NORTH COLLEGE STATION  
ATTN TRAVIS L. SIMPSON  
LUBBOCK, TX 79417

UNITED TECHNOLOGIES CORP  
HAMILTON STANDARD DIVISION  
BRADLEY INTERNATIONAL AIRPORT  
ATTN CHIEF ELSEC DESIGN  
WINDSOR LOCKS, CT 06069

WESTINGHOUSE ELECTRIC CORPORATION  
ADVANCED ENERGY SYSTEMS DIV  
P.O. BOX 10864  
ATTN TECH LIB  
PITTSBURGH, PA 15236

US ARMY ELECTRONICS RESEARCH  
& DEVELOPMENT COMMAND  
ATTN TECHNICAL DIRECTOR, DRDEL-CT

HARRY DIAMOND LABORATORIES  
ATTN CO/TD/TSO/DIVISION DIRECTORS  
ATTN RECORD COPY, 81200  
ATTN HDL LIBRARY 81100 (3 COPIES)  
ATTN HDL LIBRARY (WOODBIDGE) 81100  
ATTN TECHNICAL REPORTS BRANCH, 81300  
ATTN CHAIRMAN, EDITORIAL COMMITTEE  
ATTN CHIEF, 21000  
ATTN CHIEF, 22000  
ATTN CHIEF, 22100 (3 COPIES)  
ATTN CHIEF, 22300  
ATTN CHIEF, 22800  
ATTN CHIEF, 22900  
ATTN CHIEF, 13300  
ATTN CHIEF, 21100 (3 COPIES)  
ATTN CHIEF, 21200  
ATTN CHIEF, 21300 (5 COPIES)  
ATTN CHIEF, 21400 (2 COPIES)  
ATTN CHIEF, 21500  
ATTN BALICKI, F. W., 20240  
ATTN WIMENITZ, F. N., 20240  
ATTN TALLERICO, A., 47400  
ATTN BIKBY, R., 22900  
ATTN WYATT, W. T., 21300 (20 COPIES)